JGR Atmospheres

RESEARCH ARTICLE
10.1029/2023JD039132

The Diurnal Cycle of Rainfall and Deep Convective Clouds Around Sumatra and the Associated MJO-Induced Variability During Austral Summer in Himawari-8

Clemente Lopez-Bravo[1,2], Claire L. Vincent[1], Yi Huang[1], and Todd P. Lane[1]

[1]School of Geography, Earth and Atmospheric Sciences, The University of Melbourne, and ARC Centre of Excellence for Climate Extremes, Melbourne, VIC, Australia, [2]Now at Climate Change Research Centre, University of New South Wales, and ARC Centre of Excellence for Climate Extremes, Sydney, NSW, Australia

Key Points:

- Rainfall Potential Areas have shown semi-diurnal structures of deep convective clouds over the Indian Ocean
- An explicit sea-ward propagation pattern of deep convective clouds and complex interactions between island were found in the Java Sea
- The cloud top height reaches a maximum in the Madden-Julian Oscillation convective enhanced phase

Supporting Information:

Supporting Information may be found in the online version of this article.

Correspondence to:

C. Lopez-Bravo,
c.lopez_bravo@unsw.edu.au

Citation:

Lopez-Bravo, C., Vincent, C. L., Huang, Y., & Lane, T. P. (2023). The diurnal cycle of rainfall and deep convective clouds around Sumatra and the associated MJO-induced variability during Austral Summer in Himawari-8. *Journal of Geophysical Research: Atmospheres*, *128*, e2023JD039132. https://doi.org/10.1029/2023JD039132

Received 25 APR 2023
Accepted 18 OCT 2023

Author Contributions:

Conceptualization: Clemente Lopez-Bravo, Claire L. Vincent, Yi Huang, Todd P. Lane
Data curation: Clemente Lopez-Bravo
Formal analysis: Clemente Lopez-Bravo
Funding acquisition: Claire L. Vincent
Investigation: Clemente Lopez-Bravo
Methodology: Clemente Lopez-Bravo
Software: Clemente Lopez-Bravo
Supervision: Claire L. Vincent, Yi Huang, Todd P. Lane
Validation: Clemente Lopez-Bravo

Abstract

The effects of the diurnal cycle and large-scale atmospheric disturbances dominate rainfall and cloud variability in the Maritime Continent. This study examines the modulation of the Austral Summer diurnal cycle by the Madden–Julian Oscillation (MJO) using cloud populations through precipitation and deep convective cloud derived from satellite measurements. Using Rainfall Potential Areas from Himawari-8 Advanced Himawari Imager as a proxy for deep convection, our analysis shows that convective clouds are present ∼55% of the time over land in Sumatra during the afternoon and night. Cloud signatures reveal semi-diurnal structures of deep convective clouds off the West Coast of Sumatra. In contrast, the East Coast exhibits explicit sea-ward propagation patterns of deep convective controlled by the coastal effects around the Strait of Malacca and Java Sea, together with the influence of synchronized diurnal forcing between islands. We show that the MJO drives the enhanced convective phases, changing the cloud top type distribution, moisture convergence, and moisture transport over the equatorial Indian Ocean. The cold cloud area also increases during the MJO active phases, which is linked to frequent deep convective cloud development near the mountain ranges of Sumatra and the adjacent ocean. The analyses of cloud variations based on the rainfall potential areas and cloud top type provide evidence of the effects of convective processes on the diurnal cycle of ice and water vapor distribution in the troposphere.

Plain Language Summary

This study investigates the different weather patterns affecting rainfall and clouds in the Maritime Continent during the Southern Hemisphere summer. Potential areas of deep convective rainfall are derived from the geostationary satellite Himawari-8. We found that these clouds experience two life cycles in a single day on the West Coast of Sumatra and the open Indian Ocean, while on the East Coast, their patterns are more complex, potentially due to the influence of the surrounding islands. Additionally, we explore how those convective clouds and their properties change in relation to the Madden-Julian Oscillation (MJO), an equatorial traveling "pulse" of cloud and rainfall from west to east typically recurring every 30–60 days, during the summer season. Our results suggest that the height of the clouds reaches a maximum, and that ice cloud frequency also increases when the MJO is located over the western region of the Maritime Continent. This study contributes to understanding the effects of the MJO and convective clouds in the daily patterns of ice and water vapor in the atmosphere over Sumatra.

1. Introduction

Changes to the diurnal cycle (DC) of deep convective clouds in the Maritime Continent (MC) are the result of the daily variation in background wind flow, moisture, and incoming solar radiation (Lopez-Bravo et al., 2023; Short et al., 2019; Vincent & Lane, 2016, 2017). The diurnal changes in the amount and spatial distribution of water vapor, clouds, and wind anomalies in the MC determine rainfall distribution over the coastal regions and major islands in the MC (Bergemann & Jakob, 2016; Mori et al., 2004). Meanwhile, the strength of diurnally driven convection and rainfall linked to land-sea-breeze systems is influenced by intraseasonal sources of variability, such as the Madden-Julian Oscillation (Birch et al., 2016; Neale & Slingo, 2003; Peatman et al., 2014; Vincent & Lane, 2016).

Previous studies have explored the diurnal variability of convective clouds over the MC based on satellite-based rainfall data from the Tropical Rainfall Measuring Mission (TRMM) (Fujita et al., 2010; Kikuchi & Wang, 2008; Mori et al., 2004; Nesbitt & Zipser, 2003; Oh et al., 2012; Sakaeda et al., 2020; Teo et al., 2011; Vincent &

Writing – original draft: Clemente Lopez-Bravo
Writing – review & editing: Claire L. Vincent, Yi Huang, Todd P. Lane

Lane, 2016; Wu, Mori, et al., 2008), Integrated Multi-satellitE Retrievals (IMERG) for the Global Precipitation Measurement (GPM) (Tan et al., 2019), lightning observations (Virts et al., 2011, 2013), numerical modeling (Fujita et al., 2010; Ruppert et al., 2019; Teo et al., 2011; Vincent & Lane, 2016; Wu, Mori, et al., 2008), satellite-based infrared imagery (Fujita et al., 2010; Lopez-Bravo et al., 2023; Mori et al., 2004; Sakurai et al., 2005; Takayabu, 1994; Yamanaka et al., 2018; Yang & Slingo, 2001) and scatterometer instruments (Short et al., 2019). These studies have established the role of tropical tropospheric cloud variations driven by different physical mechanisms, and shown that the DC of clouds differs significantly between land and ocean in the free troposphere over the MC. Over the land and coastal regions, the diurnal cloud cycle is driven by convective heating at the lower levels of the troposphere and exhibits a maximum at night (Vincent & Lane, 2017). The land-sea temperature contrast generates seaward pressure gradients along the coasts of Sumatra, driving inland propagation during the afternoon (As-syakur et al., 2019; Mori et al., 2004). The DC of the convective cloud has been attributed to a thermodynamic response to a strong DC of the land surface temperature. In contrast, the physical mechanisms behind the DC of tropical convective clouds over the ocean remain poorly understood (Yang & Slingo, 2001).

The background wind conditions and intense heating along the mountain slopes forces convective initialization during the late afternoon and evening (Mori et al., 2004; Qian, 2020). However, the local circulation patterns shift during afternoon-night: subsidence is located down the mountain slopes, producing convergence and rainfall over the adjacent areas (early morning). In some regions, non-local influences have been shown after the time of the diurnally driven convective maximum. For example, the land breeze from Sumatra propagates over the Java Sea during the morning, and the cloud population from Sumatra and the Malay Peninsula converges over the Strait of Malacca near the East Coast of Sumatra, producing a frequent convective area during the night and morning hours (As-syakur et al., 2019; Birch et al., 2016; Mori et al., 2004; Vincent & Lane, 2016). In addition, inertia-gravity waves have been suggested as a mechanism of propagation of the diurnally driven convection in Sumatra (Love et al., 2011; Mapes et al., 2003; Ruppert et al., 2019; Tulich & Mapes, 2008; Vincent & Lane, 2016). The inertia-gravity waves propagate offshore, leading to the afternoon-nocturnal convective response along the coastlines of Sumatra (Ruppert et al., 2020; Short et al., 2019; Vincent & Lane, 2016).

Previous studies of the DC in Sumatra based on geostationary data used a single infrared spectral band to detect cold cloud top areas (As-syakur et al., 2019; Sakurai et al., 2005). Consequently, those studies do not include the multi-channel derived property of water vapor at different troposphere levels. In this study, we use the multi-channel derived rainfall potential areas (RPA) to improve the description of local variations of the diurnally driven convection across Sumatra.

Additionally, the two-way response between diurnally driven convection and the propagating Madden-Julian Oscillation (MJO) distances produces changes in atmospheric conditions that modulate organized mesoscale convective systems, cloud population, and rainfall over Sumatra. Rauniyar and Walsh (2011), Peatman et al. (2014), Birch et al. (2016), and Vincent and Lane (2016) demonstrate the diurnal effects of the enhanced and suppressed convective phases of the MJO in rainfall mean and anomalies over the islands of the MC. However, there have been few studies of cloud properties on a regional scale during the MJO passage over Sumatra. This is important for macrophysical, microphysical and precipitation processes, severe storms, numerical modeling, and forecasting heavy rainfall events. Here, the Himawari-8 Advanced Himawari Imager (AHI) allows us to comprehensively examination the diurnal evolution of cloudiness over land and ocean to exhaustively examine the local and regional differences under distinct weather conditions. The advanced satellite observations from Himawari-8 AHI can fill the knowledge gap and contribute to understanding the local features and retrieved cloud-top properties, including the diurnal and intraseasonal variability over Sumatra in the Austral Summer.

This study aims to characterize the DC in cloudiness and its regional differences over the MC during the Austral summer December-January-February (DJF, 2016–2021). The analysis is performed on the Austral summer period to coincide with the wet season and the increased prevalence of deep convection in the region, and for consistency with numerous other studies (Lopez-Bravo et al., 2023; Qian, 2008; Vincent & Lane, 2017). Taking advantage of the unique spatiotemporal and spectral resolution of Himawari-8 AHI, Infrared (IR) techniques, and satellite-derived cloud top properties from Himawari-8 AHI produced with the Community Satellite Processing Package for Geostationary Data, Geostationary Cloud Algorithm Testbed (CSPP-Geo GEOCAT) Level-2 version 1.0.3. Satellite-based rainfall from the IMERG V06 data collection and the European Centre for Medium-Range Weather Forecasts ECMWF Reanalysis 5th Generation (ERA5) reanalysis are utilized to examine background

atmospheric conditions relevant to the diurnal rainfall variation. We conduct a series of analyses based on geostationary satellite information in order to address the research questions of the study, which are as follows: (a) How do state-of-the-art satellite data sets provide new insights into the diurnal evolution of deep convective systems and their variation between land, coastal, and ocean regions over the western MC and the eastern Indian Ocean? (b) How does the signature of the locally driven diurnal variation of deep convective clouds relate to the development of organized convective cells and the non-local effects of synchronised diurnal forcing between Sumatra and surrounding islands? (c) How do the spatiotemporal variations in cloud top types (as derived from Himawari-8 AHI) change under the MJO-enhanced and suppressed convective phases? The observational data sets and the analysis methods used in the study are examined in Section 2. Section 3 presents the harmonic analysis of rainfall, land and ocean responses of the diurnally driven convection, local signatures of the diurnal land- sea-breeze driven propagation across Sumatra, and the diurnal variability modulation of Cloud Top Height (CTH) and cloud-top type by the MJO. Discussion and conclusions are found in Sections 4 and 5, respectively.

2. Data and Methods

2.1. The Satellite-Derived Data Set From Himawari-8 AHI

The atmospheric and cloud products derived from Himawari-8 AHI were produced using the Community Satellite Processing Package for Geostationary Data, Geostationary Cloud Algorithm Testbed (CSPP-Geo GEOCAT) Level-2 version 1.0.3 in conjunction with additional ancillary data sets. Two data sets were produced over the MC and Australia at the same satellite spatial resolution and hourly temporal resolution for DJF from 2016 to 2021: Level-1 includes the brightness temperature of 16 spectral bands of Himawari-8 AHI (Lopez-Bravo et al., 2021a) and Level-2 products provide cloud properties, for example, cloud top temperature, height, optical depth, and type with hourly temporal resolution, and 2 km horizontal resolution (Lopez-Bravo et al., 2021b). The cloud-top type product was derived from the algorithm initially developed for the GOES-R ABI instrument; after that, the algorithm was adapted to the Himawari-8/9 AHI instrument by the CSPP-Geo project. The cloud top algorithm uses infrared channels to determine cloud phases and brightness temperature differences, and effective absorption optical depth ratios are used in the spectral tests (Heidinger et al., 2020; Pavolonis, 2010). In this work, three cloud-type categories are presented. Optically thin ice clouds: ice clouds with an infrared optical depth $\leq\sim2.0$; Optically thick ice clouds: clouds with high emissivity ice topped clouds, for example, those with infrared optical depths >2.0, and Multilayered clouds: clouds which are optically thin ice clouds overlapping a lower optically thick cloud layer (Pavolonis, 2010). Data sets and the complete list of variables are available at National Computational Infrastructure, Australia (Lopez-Bravo et al., 2021a, 2021b). The hourly data set was used to characterize large-scale drivers over the MC during the six Austral summers of DJF from 2016 to 2021. A multi-threshold post-processing method was further implemented to remove pixels that are subject to significant uncertainties and retrieval artifacts (Huang et al., 2019; Lopez-Bravo et al., 2023). Note that the observation period includes the influence of the interannual variability from El Niño-Southern Oscillation (ENSO; El Niño: 2014–2016 and 2018–2019; La Niña: 2017–2018 and 2020–2021) and the Indian-Ocean Dipole (IOD; IOD+: 2019; IOD-: 2016, 2020, and 2021), which has been explored by Hamada et al. (2002, 2008) and Qian (2020).

2.2. IMERG Data Collection

The satellite-based rainfall from the IMERG V06 precipitation rate ("precipitationCal") data is used to explore the diurnal rainfall over Sumatra. The IMERG data set is currently the most advanced remote sensing precipitation product (G. Huffman, Bolvin, et al., 2019; G. Huffman, Stocker, et al., 2019; G. J. Huffman et al., 2020; Yu et al., 2022). The IMERG algorithm intercalibrates, merges, and interpolates microwave precipitation estimates from the Global Precipitation Measurement satellite constellation, integrating microwave-calibrated infrared satellite estimates and precipitation gauge data to produce a global-gridded data set with spatiotemporal resolutions of 0.1° and 30-min resolution (G. Huffman, Bolvin, et al., 2019; G. Huffman, Stocker, et al., 2019; G. J. Huffman et al., 2020). This study uses hourly precipitation estimates during the Austral summer DJF from 2001 to 2021 as a regional reference for the DC due to its climatological/monthly calibration to gauge-based products that reduces the uncertainties in the satellite-derived diurnal precipitation means over the land. Tan et al. (2019) and Da Silva et al. (2021) showed the performance of IMERG in capturing the DC over the MC. The DC of precipitation based on IMERG is consistent with previous investigations of the DC in the MC where ground observations, satellite-derived rainfall, and active retrievals were used (Kikuchi & Wang, 2008; Mori et al., 2004;

Qian, 2008; Rauniyar et al., 2017; Vincent & Lane, 2016; Worku et al., 2019). However, orographic and coastal biases in the IMERG data set have been documented, such as diurnal amplitudes overestimated over the central region of the United States (US) and underestimated over areas of complex topography in the US (Sungmin & Kirstetter, 2018; Tan et al., 2019; Watters et al., 2021). Similar underestimations and poor performance have been documented over the mountain ranges and coastal regions in Europe (Navarro et al., 2019; Tapiador et al., 2020). The MC exhibits both conditions, complex coastlines, and topography. In addition, ground-based and upper-level observations are limited over land and ocean to validate the satellite-derived products. For these reasons, the satellite-derived estimation of deep convective clouds based on Himawari-8 AHI provides an ideal data set to characterize the diurnal and sub-diurnal structures of the tropical deep convective system at a finer resolution that IMERG over the land and coastal regions in the MC.

2.3. Rainfall Potential Area

Based on the concept that deep convection penetrates the tropical tropopause layer and changes water vapor content in the lower stratosphere, the overshooting cloud tops are used as a proxy of deep convective clouds associated with the diurnally driven convection propagating offshore Sumatra (Hassim & Lane, 2010; Lopez-Bravo et al., 2023). This work uses geostationary measurements from Himawari-8 AHI sensor to analyze deep convective clouds based on the tropopause temperature and convective overshooting using the water vapor and infrared channels.

Brightness temperature (BT) from Himawari-8 AHI is used for detecting deep convective clouds based on infrared bands: 6.2, 10.4, and 12.4 μm. The identification of the RPAs follows JMA (2015) with the detection of high cloud tops near the tropopause and convective overshooting according to the following criteria:

1. 6.2 μm BT ($BT_{6.2}$, K) < 10.4 μm BT ($BT_{10.4}$, K) and 12.4 μm BT ($BT_{12.4}$, K): Developing clouds with tops below the level of the tropopause.
2. $BT_{10.4} \sim BT_{6.2} \sim BT_{12.4}$: Deep convective clouds reaching the tropopause
3. $BT_{6.2} > BT_{10.4}$: Overshooting cloud top intrusion through the level of neutral buoyancy near the deep convective areas in the lower stratosphere
4. $BT_{10.4} > BT_{12.4}$: Thin cirrus clouds, which are removed from the scene, as they are not associated with deep convection.

After identifying the RPA (criteria 2 and 3) associated with deep and cold cloud systems, subareas of the RPAs were identified and labeled in each scene by applying a segmentation method based on the watershed algorithm (Beucher, 1979; Heikenfeld et al., 2019). The segmented areas of the RPAs were used to estimate the probability of detection (POD) and false alarm ratio (FAR) between the RPAs and the rainfall estimates from IMERG. The POD for the RPA and rain rate above 0.1 mm hr^{-1} is 86% and the FAR is 18%, determined by regridding the RPA to the coarse resolution of the rainfall estimates from IMERG V6. The reported value is consistent with a previous evaluation from JMA (2015). Additionally, the labeled RPAs were employed to explore the diurnal signatures of deep convective clouds over Sumatra, the IO, and the internal seas of the MC at 2 km spatial resolution (Himawari-8 AHI).

2.4. Section Analysis of Sumatra

The mountain ranges over the western region of Sumatra and the lowland in the eastern portion of Sumatra are essential elements in generating a local-scale diurnal circulation of the land-sea and mountain-valley breeze system. Studies have shown that the diurnal wind anomalies tend to be perpendicular to the coastline and mountain ranges in Sumatra (e.g., Short et al., 2019), and potential temperature anomalies associated with the land-sea-breeze system have been shown to follow a similar pattern related islands in the MC region such as New Guinea (Vincent & Lane, 2016). Although the propagation of individual clouds and convective systems is inhomogeneous due to the geographical location of Sumatra over the equator and the influence of Borneo, Java, and the Malay Peninsula (Lopez-Bravo et al., 2023; Ruppert et al., 2020), the aggregated propagation of the cloud population is assumed to be perpendicular to the coastlines in most cases. To explore the offshore propagation of cloud populations:

1. Five control areas have been chosen, one over land Sumatra area and four parallel bands extending over the Indian Ocean (IO) from the West Coast of Sumatra, with an average perpendicular distance of 240 km from the coastline in each band.
2. Multiple sections approximately perpendicular to the West Coast of Sumatra (WCS) and the mountain ranges were extracted using 2 km spacing between sections in order to keep the same spatial resolution as Himawari-8

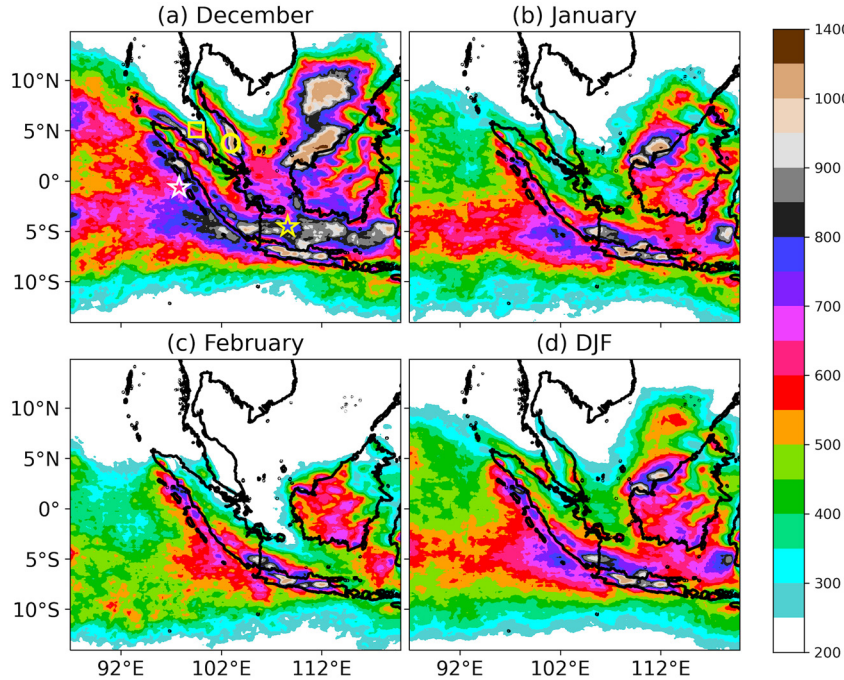

Figure 1. Spatial distribution of monthly accumulated precipitation (mm) of observed seasonal precipitation by IMERG for Austral summer December-January-February (DJF, 2001–2021). (a) December, (b) January, (c) February, and (d) the average monthly accumulated precipitation for DJF. Geometric shapes in panel (a) indicate geographical locations. Yellow star: The Java Sea, yellow circle: The Malay Peninsula, yellow square: The Malacca Strait, and white star: The West Coast of Sumatra.

AHI. After that, the sections were grouped and averaged into six bands across Sumatra every ~240 km. Additionally, zonal sections were computed over the southeastern region of Sumatra near the Java Sea.

2.5. Reanalysis Data ERA5

The European Centre for Medium-Range Weather Forecasts (ECMWF) Reanalysis 5th Generation (ERA5) data are used to compute composite analyses of zonal and meridional wind components. First, wind components were vertically averaged over the 925–850 hPa for Austral summer from 2016 to 2021 by MJO phases. Similar composite analyses were performed for the vertically integrated moisture divergence from the surface of the Earth to the top of the atmosphere (VIMD, kg m^{-2}), and streamlines to verify the effects of the enhanced and suppressed convective phases of the MJO over the large-scale patterns and moisture availability. The evolution and strength of the MJO are frequently represented by the Real-time Multivariate MJO (RMM) index (Wheeler & Hendon, 2004), which is based on the first two EOFs of a multivariate field composed of zonal wind in the lower troposphere (850 hPa) and upper level (200 hPa), and OLR. The MJO phases were selected by the RMM index, filtering the date when the amplitude of the RMM index was greater than or equal to 1 to include significant MJO events.

3. Results

3.1. Austral Summer Rainfall DJF

The MC is one of the most favorable regions for frequent deep convective activity and rainfall in the tropics, but this activity is by no means homogenous across the region. Figure 1a shows the distribution of accumulated rainfall from IMERG in the western MC in December. During the Austral summer, Sumatra exhibits a wide spatial variation in rainfall over the land and ocean. The differences in rainfall vary according to seasonal changes and are affected by the migration of the Intertropical Convergence Zone (ITCZ) toward the southern hemisphere during the months of December, January, and February. The maximum rainfall is observed in the southwest and offshore of Sumatra. Well-defined spatial patterns are also seen over the Strait of Malacca (yellow square in Figure 1a), the

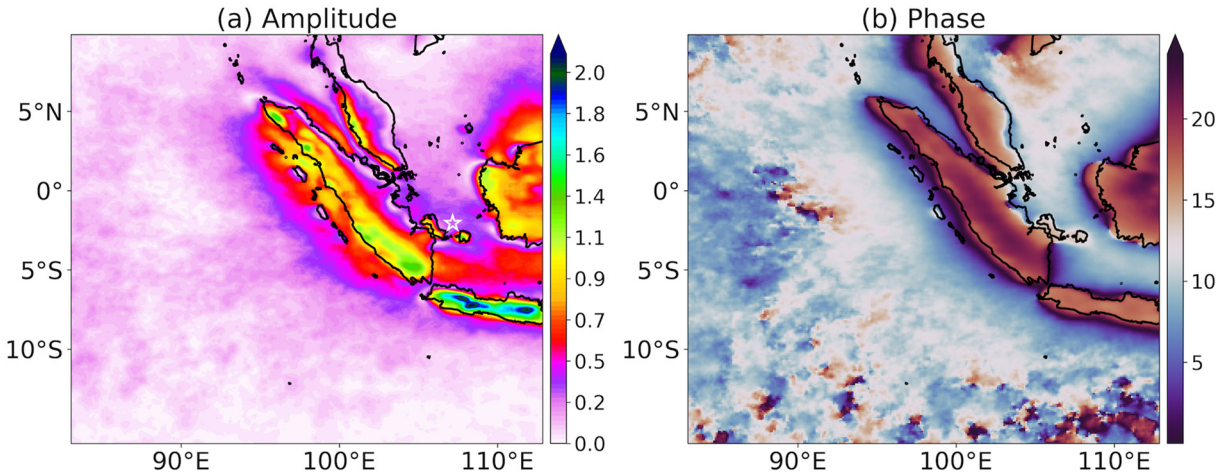

Figure 2. Harmonic analysis from IMERG data. Shaded colors indicate: (a) The amplitude, and (b) the time of the phase of the precipitation maximum peak (LST UTC+7 for Sumatra phase) of the first harmonic of the DC for DJF over 2001–2021. The white star indicates the location of the Bangka-Belitung Islands in panel (a).

WCS (white star in Figure 1a), and the Java Sea (yellow star in Figure 1a). The rainfall signature shifts southward during the evolution of the Austral summer, decreasing the amount of rainfall over the Malay Peninsula (yellow circle in Figure 1a), the Strait of Malacca, and the IO region over the northern hemisphere (Figure 1b). The region between 13°S and the equator shows a clear zonal band of rainfall associated with the seasonal migration, position and structure of the ITCZ, the Asia-Australian monsoon, and persistent circulations over the southern IO (As-syakur et al., 2019; Murakami & Matsumoto, 1994; Qian, 2020; Sakurai et al., 2005). Additionally, the seasonal southward progression of rainfall affects the storm features on the East Coast of Sumatra and the Malay peninsula and the Strait of Malacca, which become progressively more suppressed from December to February (Figures 1a–1c). Note that the pattern of monthly accumulated precipitation is actually the aggregate contribution of individual convective systems in the MC, and is especially sensitive to the diurnal activity over the archipelago of islands in the MC and interactions with surrounding oceans (As-syakur et al., 2019; Hamada et al., 2002; Qian, 2020; Sakurai et al., 2005; Yamanaka et al., 2018).

3.2. Estimation of the Amplitude and Phase of the Diurnal Cycle

The amplitude and phase of the DC are obtained based on harmonic analysis of satellite-derived precipitation from IMERG. The method is comparable with the TRMM 3B42 analyses in Rauniyar et al. (2017) and Sakaeda et al. (2017, 2020). Fourier analysis is used to calculate the amplitude and phase of diurnal harmonics. The phase of the diurnal harmonic indicates the local time of maximum value. Figure 2 shows the diurnal amplitude, and the Local Standard Time (LST UTC+7 for Sumatra) of the rainfall peak (phase) during 2001–2021. Diurnal amplitudes of rainfall with values > 0.5 mm hr^{-1} are found over the major islands and their surrounding oceans in the western region of the MC. The largest amplitudes tend to be located over Sumatra, Java, Borneo, and the West Coast of the Malay Peninsula. The maximum amplitude in Sumatra follows the mountain ranges over the western region with an inhomogeneous pattern along the coastline. The offshore coastal area shows three relevant regions with high amplitude values: an area within the first 200 km from the WCS over the IO, the Strait of Malacca, and the Java Sea. Amplitudes <0.3 mm hr^{-1} over the eastern equatorial IO, the interior seas of the MC, and regions over the East Coast of Sumatra indicate a weaker average DC.

The coastal diurnal activity shows differences between northern and southern Sumatra (Figure 2b), which are dictated by the longitude difference between west and east Sumatra (~10°). The zonal distance gives ~40 min of difference in solar noon; this could explain some of these observed differences. The maximum precipitation occurs at approximately 21:00 LST over the region near the mountains in central-southern Sumatra. This finding is consistent with that of (As-syakur et al., 2019; Mori et al., 2004; Sakurai et al., 2009) who explored the rainfall and component of evening convergence and over landmasses. The peak in northern Sumatra occurs earlier at around 18:00–20:00 LST. Note that the peak over the northern Sumatra region is located over the land and the WCS. The morning rainfall is identified over the coastal sea regions surrounding the islands. The southwestern coastline of Sumatra, the Strait of Malacca, and the Java Sea present a strong contrast between the evening rainfall

over land regions and the morning rainfall in the coastal sea regions. However, the time of the maximum peak of the DC in the far-offshore eastern IO (Latitude 6°S to 4°N and Longitude 85°E) is approximately in phase with that over the coastal area over the WCS. Short et al. (2019) noted a similar onset of non-propagating variations near-surface wind speed in this region. This raises the question of whether propagation systems influence the DC in this region from the land or a separate process relating to the oceanic DC. In the next section, the structures of deep convective cloud based on the higher-resolution RPA from Himawari-8 AHI are analyzed to explore the convective contribution of rainfall linked to the land-and sea-breeze systems in Sumatra.

3.3. Propagation of the Diurnally Driven Convection Based on the RPA

We assume that most of the total rainfall comes from convective processes over the MC (Dion et al., 2019, 2021), and therefore use the RPA to characterize the variation at the diurnal scale. This approach is also justified by the fact that the heaviest rain leads to extreme rainfall rates, and flooding is associated with deep convective rainfall. The number of occurrences of RPA over six Austral Summers (540 days) is shown in Figure 3 at 2-hourly time intervals through the day. The maximum frequency of RPA is located along the western region of Sumatra after 17:00 LST. The highest frequency RPA propagates inland and covers most of Sumatra at 19:00 LST, being more active in the western region than the East Coast of Sumatra. The frequency of the RPA shows a local variability across Sumatra, demonstrating the relevance of the effect of topography and local circulations involved in the development of the cloud population and the regions of convective initialization.

The enhanced convective areas are generated over the coastal region along the southwestern coastline between 17:00 and 23:00 LST. The RPA over the coastal sea region increases in frequency from 23:00 to 07:00 LST. Four areas are identified where the RPA presents important differences as indicated by the numbers in the 07:00 panel: (a) the near-offshore region off the WCS shows intense deep convective activity and is locally influenced by small islands located approximately 200 km from the coast (small islands near the white star in Figure 1a), showing diurnal and semi-diurnal variations: early afternoon (rectangle in Figure 3e) and early morning (rectangles in Figures 3j–3l). Note that the largest of this collection of islands off WCS have areas >5,000 km^2, which is above the critical size of 315 km^2 for developing a diurnal cycle suggested by Sobel et al. (2011, 2013). (b) The Java Sea area is diurnally driven by land-sea-breeze convective contributions from Sumatra, Java, and Borneo. (c) A region of the East Coast of Sumatra near Singapore shows cloud families propagating during the afternoon-night, and (d) the Strait of Malacca features a maximum associated with the cloud population propagating between Sumatra and the Malay peninsula, which is consistent with Fujita et al. (2010). However, the result reveals complex patterns over the Strait of Malacca that early studies could not identify due to the limited resolution of satellite-based products. These regions exemplify the non-local diurnal influences in the region. Evidently, the diurnal cycle is comprised of the interaction of multiple processes. To explore these influences over the southwestern region of Sumatra, we next examine the diurnal variation of cloud populations by calculating the fraction of cloud linked to the diurnally driven convection with increasing distances from the coast.

3.4. RPA Fraction Analysis Over Sumatra and Indian Ocean

The mean RPA fraction is calculated for six Austral summers (DJF: 2016–2021) to characterize the ocean and land in Sumatra. The cloud variations of the deep convective population are computed as the area fraction of the RPA over five selected areas over Sumatra and the IO. The RPA fraction analysis in Figure 4 shows the mean signature over the area of interest. Those areas were selected by considering the mean propagation of the cloud populations offshore Sumatra. The first propagation pattern of the diurnally driven convection, which is the slow speed component, follows the coastlines of Sumatra [NW direction of the West Coast of Sumatra (WCS)]. The cloud population develops parallel to the coastlines within the 200–300 km range over the IO. Therefore, areas were chosen to be parallel to the WCS to ensure consistency with the primary direction of propagation of cloud populations. The DC over Sumatra exhibits approximately 55% RPA fraction during the afternoon and evening (dotted gray line in Figure 4a, ~17:00–01:00 LST). However, a change in convective cloud cover between 13:00 and 23:00 LST shows the effects of the intercoastal activity and RPA propagating inland from the East and West Coasts of Sumatra, converging over the mountain ranges of Sumatra (as will be discussed later), as also seen 17:00–23:00 LST in Figure 3. After the cloud population propagates offshore Sumatra, the RPA fraction decreases, reaching a minimum of around 11:00 LST before a new convective initiation develops.

The solid salmon line in Figure 4a indicates an area within the first 220 km from the WCS over the IO; the RPA fraction shows the progression of the DC offshore Sumatra. The cloud population arrives at night with an

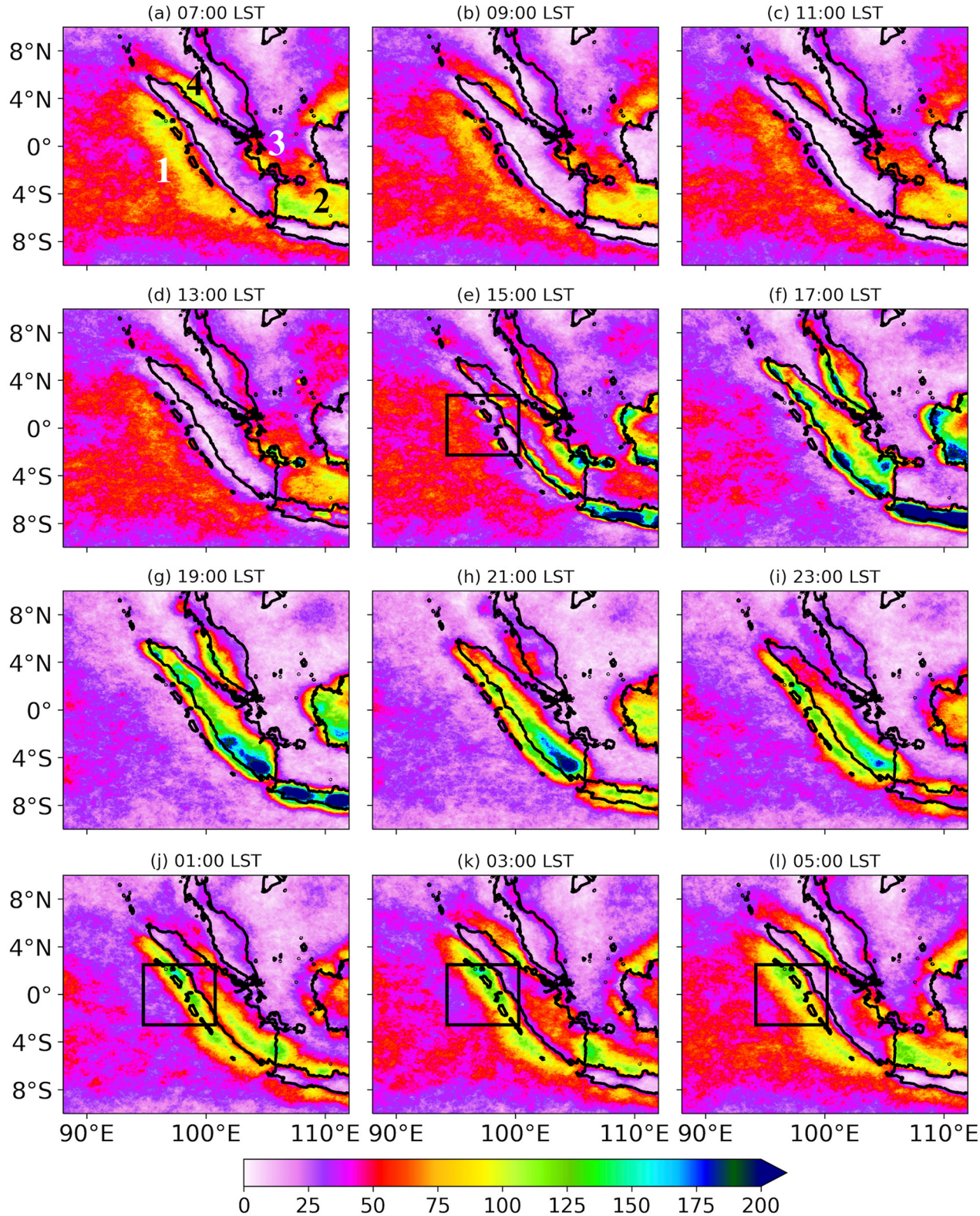

Figure 3. The spatial distribution of the number of days is presented in shaded colors. The Rainfall Potential Areas (RPA) derived from Himawari-8 AHI were calculated over six Austral summers (DJF, 2016–2021) and are presented at a 2-hourly interval time through the diurnal cycle. Numbers in the first panel refer to features discussed in the text. The rectangles in panels (e and j–l) show the semi-diurnal variation of the RPAs over small islands off the WCS.

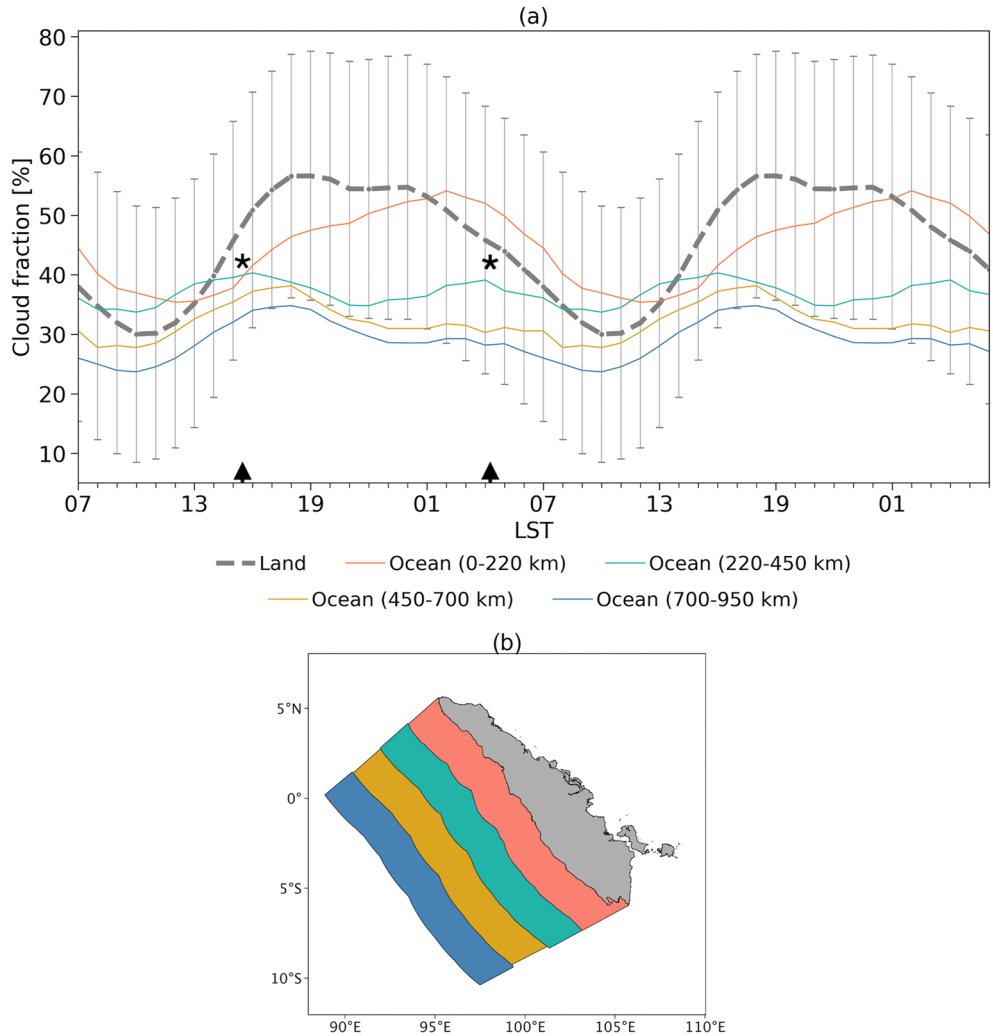

Figure 4. Analysis of RPA fraction from Himawari-8 AHI. (a) The dashed line indicates the signature over Sumatra, and error bars indicate the standard deviation over land. The solid lines show the RPA fraction of parallel bands from the West Coast of Sumatra over the Indian Ocean: Salmon line (coastal, 0–220 km), cyan line (220–450 km), gold line (450–700 km), and the blue line (700–950 km). Two weak peaks between 01:00–07:00 LST and 13:00–19:00 LST are extended almost horizontally over 300–2,000 km from the WCS. These semi-diurnal effects are indicated with the asterisks and black arrows. The plot is duplicated in the time dimension for clarity. (b) Areas associated with color lines in panel (a) over land in Sumatra and the eastern IO.

equivalent variation in RPA fraction to the land category, indicating a strong coastal activity dependency over the transition zone between land and ocean. Here, a coastal concentration of clouds and rainfall over the sea-side is inferred and supported by Figure 3 and Ogino et al. (2016). The DC in this region appears similar to that over the land, with a time lag of about 6–8 hr, depending on background wind flow conditions, indicating a translation of the land-based convection to the near coastal offshore region. The transition area shows local signatures driven by diurnally forced convection over the larger of the group of islands situated approximately 110 km off the WCS, (near the white star in Figure 1a). The RPA fraction has an inflexion point, coinciding with the diurnal maximum over Sumatra. However, these islands also exhibit a sub-diurnal contribution when the convective envelope from Sumatra propagates over the small islands ~8 hr later. Rainfall from IMERG data showed the same double peak pattern (not shown).

The solid cyan, gold, and blue colors represent the DC over the ocean between 220 and 950 km. The ocean signature shows two main features: (a) The convective envelope is found early in the morning between 220 and 450 km from the WCS (solid cyan line in Figure 4a) with a reduction of 13% of RPA fraction compared to the

land signature. Note that the cyan line is the only region with a strong semi-diurnal frequency of deep convective clouds, which appears as a combination of the offshore diurnal cycle and the propagating diurnally driven convection from Sumatra. This semi-diurnal signature with distance >200 km from the WCS shown in Figure 4a enhances our understanding of convective signatures over the IO. In contrast, the ocean signatures with distances greater than 450 km exhibit a weak DC (solid gold and blue lines). (b) RPA fraction increases quickly at noon over all areas analyzed. The DC over the ocean indicates an active phase of the DC, persisting for 7 hours around 19:00 LST. However, the RPA fraction reduces quickly due to the local DC taking over the propagating signal from land. As we move farther offshore, the signature of the propagating DC signature vanishes, and the variability becomes dominated by the local DC. The competing influence of the propagating DC from the land and the local DC manifests as reduced diurnal variability in the cyan region. This is also seen in Figure 2a, where there is a region of reduced diurnal amplitude around 90°E with a slight increase in amplitude farther west.

3.5. Local Signatures of the Diurnal Cycle of the RPA

Hovmöller diagrams of the spatial averaged RPA frequency are shown in Figure 5. This result indicates that the diurnally driven convection across Sumatra controls the local signatures. However, the DC signatures are influenced by external and complex effects from the DC of the Malay Peninsula (Figures 5a and 5b), Singapore (Figure 5c), Borneo (Figures 5d and 5e), and Java (Figure 5f). For example, the local diurnal signatures of the diurnally driven convection across Sumatra tend to develop in synchrony over the eastern IO, Strait of Malacca, and Java Sea, with a strong influence of the DCs of the Malay Peninsula, Borneo, Java, and surrounding seas. In particular, the wind over the Strait of Malacca has been a focus of early studies that describe the links between local effects of wind called "Sumatras" and severe weather conditions that affect rainfall patterns and induce changes in ocean circulations due to wind stress at the surface level associated with storm activity (Nieuwolt, 1968; Scott, 1956). Additionally, early convective initialization over the small islands provides evidence of the influence by land heating processes and the synchronised diurnal effect forced by the major islands of the MC, for example, Bangka-Belitung Islands, white star in Figure 2a, which are situated off the southeastern coast of Sumatra.

Note that these figures are long-term averages, and these effects are not always present, depending on the background wind direction and meridional differences from North to South Sumatra. Convective systems are primarily triggered over land during the afternoon. Here the RPA reaches the maximum frequency in the evening over the mountain ranges of Sumatra around 00:00 LST, as seen in Figure 5d. Panels a and b in Figure 5 show an early peak over the east coast of the Malay Peninsula and Sumatra (17:00–22:00 LST), and the sections over southern Sumatra show eastward and westward propagation simultaneously (over land), which demonstrates the intercoastal activity (Figures 5c and 5d). Additionally, a peak of RPA propagates from the WCS toward the IO during 17:00–07:00 LST as shown in Figures 5a–5d.

The propagation over the IO changes in character from the North to South of Sumatra, showing a reduced propagation speed and reduced propagation distance in the South of the island relative to the North (Figures 5a–5f). Those changes can be associated with changes in the speed and direction of the cloud populations propagating over open ocean and the regional effects of quasi-stationary circulations in the extratropical region over the IO that drives the inter-hemispheric circulation between the IO in the South and the western region of the MC. In addition, the result of the semi-diurnal signature found in Figure 4 is also observed in Figures 5a and 5b.

Hovmöller diagrams of meridionally averaged RPA frequency over the Bangka-Belitung Islands and the Java Sea are presented in Figure 6a. Interestingly, zonally propagating diurnal RPA signatures between Sumatra and Borneo show a mean speed of propagation of ∼20 m s^{-1}, which is consistent with the diurnal-phase gravity waves coupled with diurnal mesoscale convective systems in the MC (Short et al., 2019; Vincent & Lane, 2016). Additionally, the RPAs provide evidence that the offshore propagation off Borneo influences the convective initialization around the Bangka-Belitung Islands at 15:00 LST, as illustrated in Figure 6a. Note that the smallest islands (<315 km^2) do not exhibit a significant enhancement of deep convective clouds (Sobel et al., 2011, 2013). This interesting result indicates that the pattern over the Bangka-Belitung Islands can be explained as a combined effect between the Borneo convective signatures and early morning atmospheric disturbances propagating eastward over South Sumatra. The diurnal effect generates convergence over the Bangka-Belitung Islands region, which can favor the development of the DC of the next day. Figure 6b presents the average over the Java Sea to exemplify the complexity of the interaction between the DCs of Sumatra, Java, and Borneo. This finding adds a

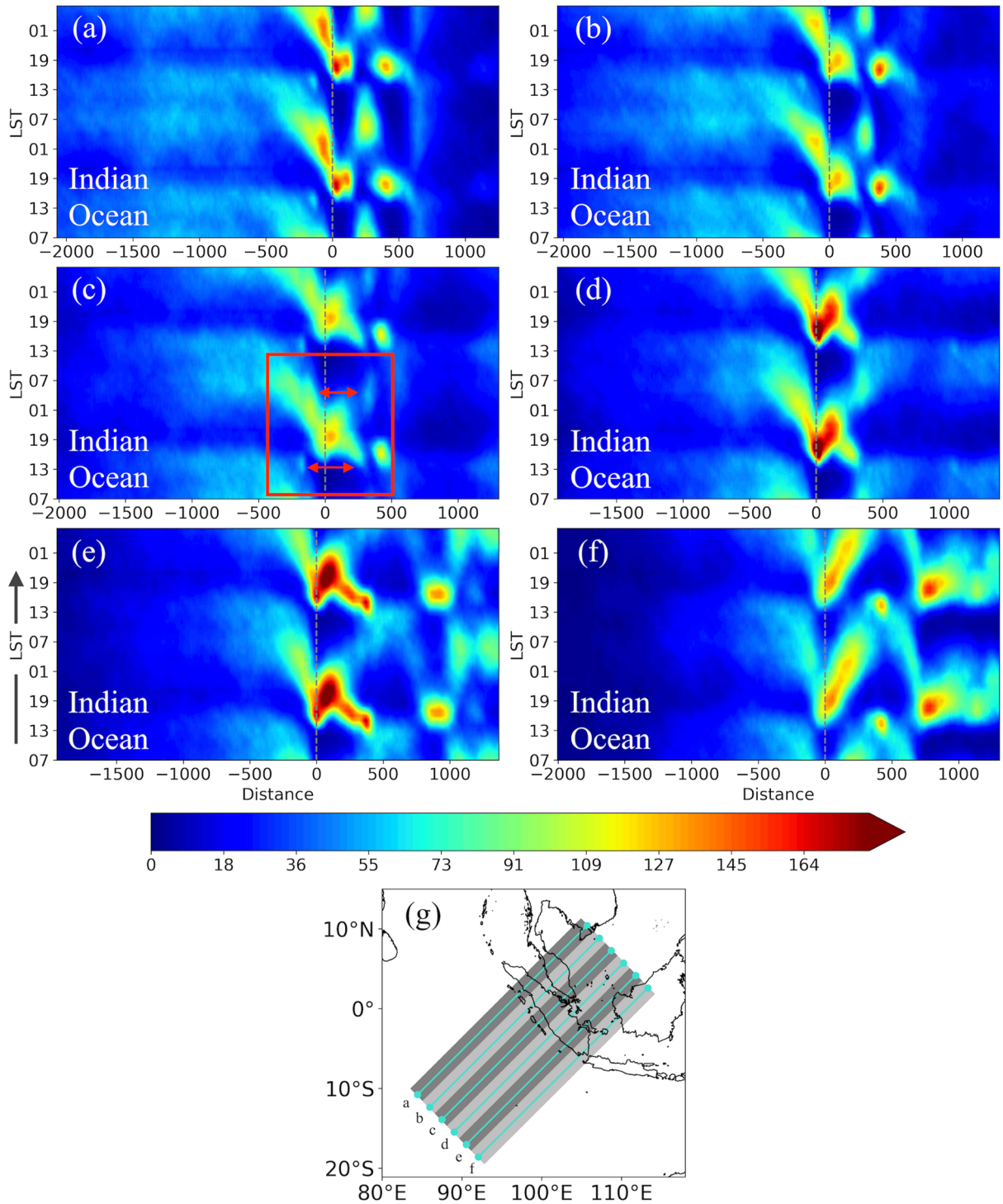

Figure 5. Hovmöller diagram of the number of days (shaded) of the RPA (DJF, 2016–2021). (a–f) Local signatures are presented by averaging perpendicular sections to the West Coast of Sumatra over the gray and light gray areas in panel g. The solid cyan lines indicate the section shown from (a to f). The thin dashed gray line indicates the West Coast of Sumatra in each panel. The red arrows and rectangle in panel c indicate the semi-diurnal signatures off Sumatra. The *Y*-axis (24 hr) has been duplicated to show the diurnal patterns.

new dimension to the understanding of synchronized diurnal cycles by showing an explicit seaward propagation of the DC of deep convective clouds over the Java Sea. The propagation of diurnally driven convection starts offshore from the East Coast of Sumatra and continues toward the Java Sea, controlling the spatial distribution of

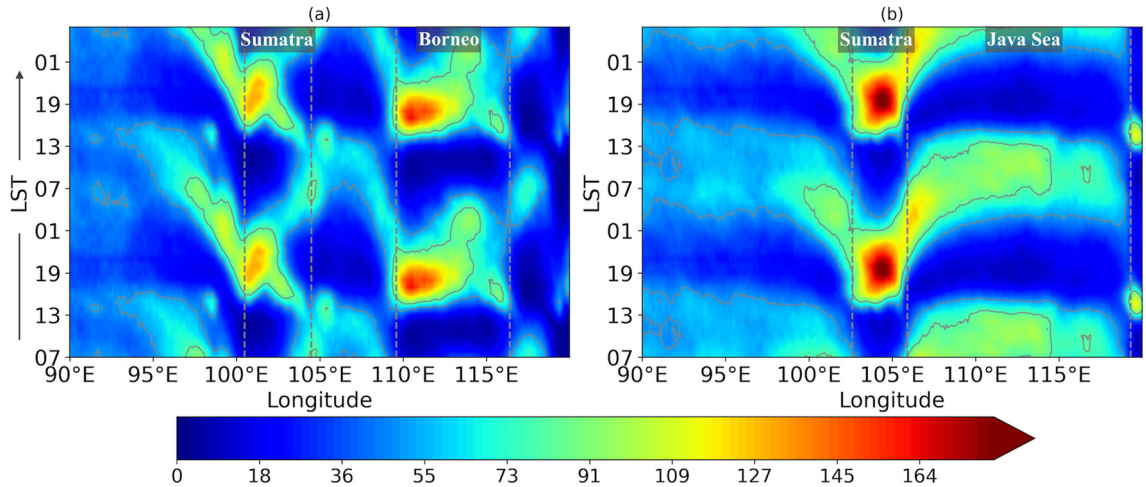

Figure 6. As in Figure 5, but Hovmöller diagram of zonal section based on Himawari-8 AHI (Longitude 90°E to 120°E). (a) Sumatra-Borneo patterns (averaged over the latitude band 2°S–0°). The dashed lines indicate the East (left) and West coast (central) of Sumatra, and the West coast of Borneo (right), (b) Sumatra-Java-Borneo patterns (averaged over the latitude band 6°S to 4°S). The dashed lines indicate the East (left) and West Coast (central) of Sumatra and the West coast of South Sulawesi (right).

the RPA in the first 200 km offshore from Sumatra. Distances greater than 200 km indicated a transition, where the DCs of Java, and Borneo control the propagation of deep convective clouds over the Java Sea. While the analysis thus far has shown the fine-scale spatial and diurnal variations in the RPAs, multiple studies have shown significant variations in both dynamical and thermodynamical aspects of clouds in the MC on intraseasonal scales (Birch et al., 2016; Kamimera et al., 2012; Peatman et al., 2014, 2021; Vincent & Lane, 2016, 2017). In the next section, we examine the variation in cloud populations on and around Sumatra with the MJO phase. Our investigation provides new insights of the diurnal variations of the cloud populations based on the cloud top type and its implications in the DC of ice in the troposphere from an MJO perspective.

3.6. MJO Cloud Variability

In this study, each day of the Austral summer between 2016 and 2021 has been assigned to one of the eight MJO phases based on the RMM index, extracting the date where the RMM index amplitude was greater than or equal to 1 (164 days of the total data period). In addition, composite analyses were generated for days during phases 6-7-8-1 (which we refer to as the MJO-suppressed convective phases over the MC) and 2-3-4 (enhanced convective phases over the MC). Movie S1 shows the diurnal brightness temperature composites based on channel 13 (10.4 μm spectral band) from Himawari-8 AHI (DJF, 2016–2021) for each phase of the MJO. The cold and shaded colors show cloud tops linked to diurnally driven convection over Sumatra and surrounding islands. Note that the MJO-enhanced convective phase shows a large cloud cover over land from 07 to 19 LST. During MJO-suppressed convective phases, convective clouds over the Indo-Pacific warm pool show less cold cloud area (cold colors) and a weaker diurnal variation. The diurnally driven convection signature shows cold cloud tops within the coastal region (distance ~250 km from the coastline).

Composites of the daily Cloud Top Height (CTH) and cloud-top type by MJO phase are shown in Figures 7 and 8, respectively. Figure 7a shows the distribution of the analyzed days in each Austral summer and phase of the MJO, representing approximately 11,200 total samples (hourly resolution). Extensive cloudiness is observed over the major islands in the MC during all MJO phases, and the composites of CTH over land in Sumatra show two different CTH values over the northern (land area with latitude to the north of the equator) and southern (land area latitude to the south of the equator) regions of Sumatra (Figure 7b). The most significant CTH differences were found at noon before the convective initialization started over the land. Clouds linked to diurnally driven convection reach a maximum between 11.5 and 12.3 km depending on the enhanced convective phases (MJO: 2, 3, and 4) or suppressed convective phases (MJO: 6, 7, and 8) of the MJO over the western region of the MC, but the differences also respond to the seasonal variability with the influence of the Intertropical Convergence Zone (ITCZ) migration toward the southern hemisphere during the DJF months.

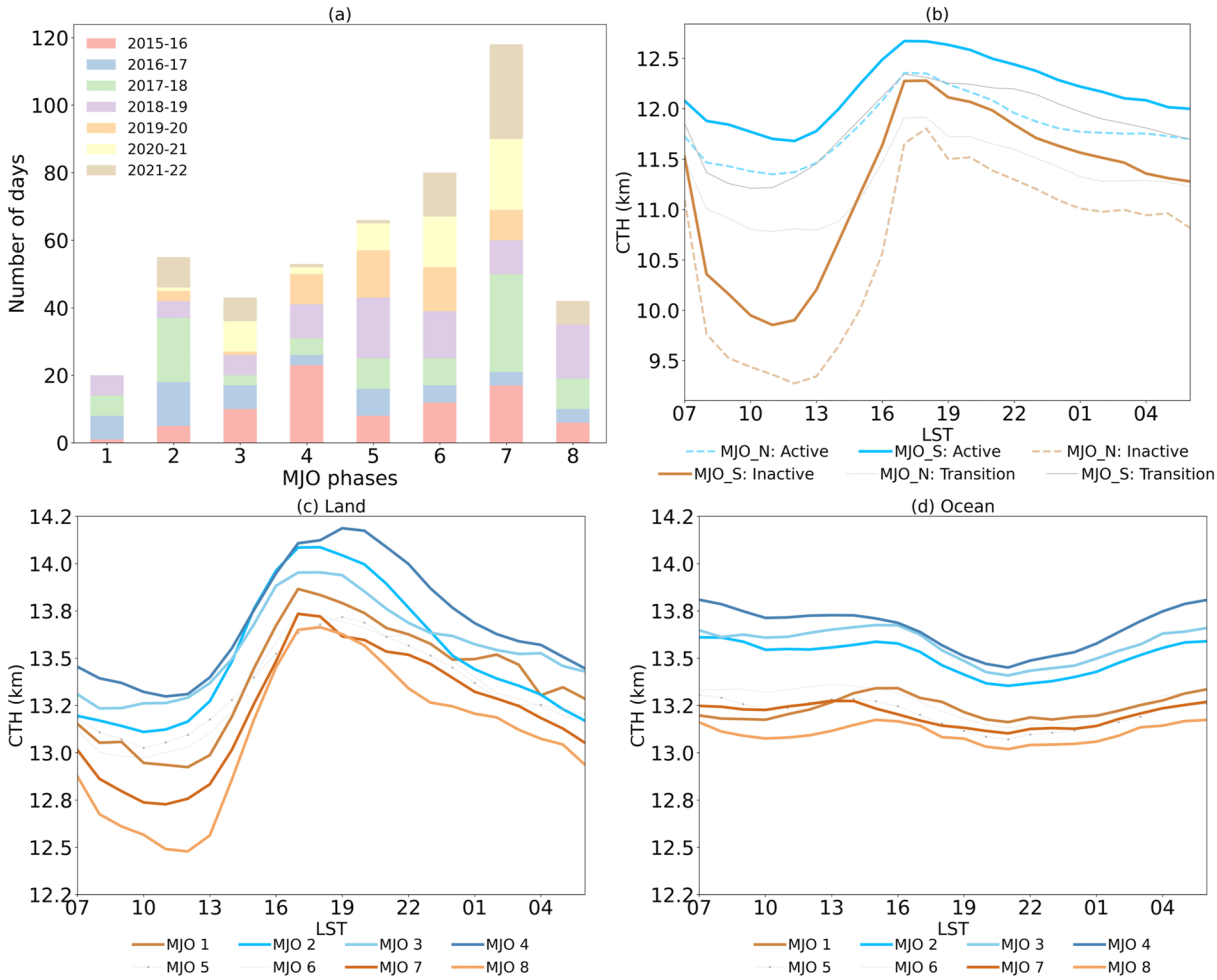

Figure 7. Composite analysis of the Cloud Top Height (CTH) by MJO phases. (a) Histogram of the number of days analyzed from the RMM index by MJO phase and Austral Summer (DJF, 2016–2021). Mean values of composite analysis from phases 1 to 8: (b) the CTH from Himawari-8 AHI, CSPP-Geo GEOCAT, and the RPA over land, the solid line indicates the selected area over south Sumatra, and the dotted line shows the northern region of Sumatra: Active phases (MJO: 2-3-4), Inactive phases (MJO: 7-8-1), and Transition phases (MJO: 5–6). The CTH signatures were identified by the MJO phase during DJF (c) the 90th percentile of the CTH over land Sumatra and (d) the 90th percentile of the CTH over ocean.

The land and ocean CTH signatures were calculated over Sumatra and surrounding waters. Figures 7c and 7d show the 90th percentile of CTHs. Diurnally driven convection is consistent through all phases of the MJO, but we note the following variations:

1. The highest CTHs are found in the enhanced convective phases (2-3-4) over both land and water.
2. The MJO has a strong modulation of CTH between 07 and 13 LST.
3. Over the ocean, there is a weaker diurnal variation in CTH over the ocean than over the land. However, the ocean diurnal variation appears more pronounced (larger amplitude) during the MJO-enhanced convective phases (MJO: 2, 3, and 4).

These results are consistent with locally driven convection during the MJO-suppressed convective phases and large-scale forcing for convection during the MJO-enhanced convective phases and demonstrate that the enhanced diurnal cycle ahead of the MJO onset is not necessarily linked to deeper convection and rainfall. According to research by Peatman et al. (2014), Birch et al. (2016), and Vincent and Lane (2017), the highest intensity of rainfall occurs over land in Sumatra during the MJO Phase 2 (ahead of the convective phase of the MJO). This finding complements those previous studies and presents evidence that the deepest CTHs tend to occur more frequently over the ocean and land in Sumatra during the MJO Phase 4.

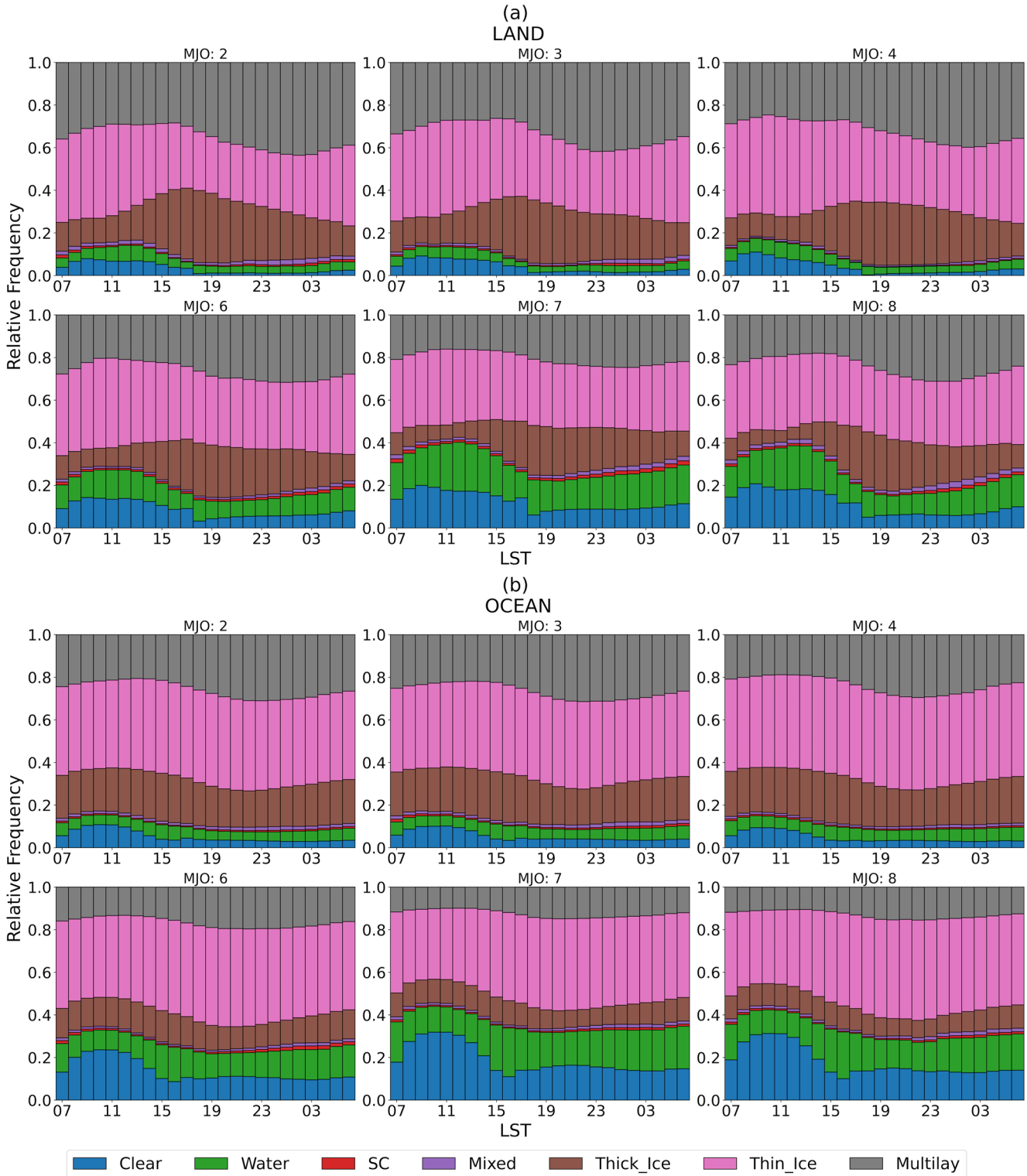

Figure 8. Relative frequency histograms show a composite analysis of cloud top type by MJO phase. Cloud top type is derived from Himawari-8 AHI (Lopez-Bravo et al., 2021b). (a) Land and (b) ocean. Colors indicate the cloud top type. Blue: Clear, Green: Water, Red: Supercooled, Purple: Mixed, Brown: Thick ice, Pink: Thin ice, and Gray: Multilayer.

Composite cloud top types derived from Himawari-8 AHI showed a diurnal and MJO-scale variation in all categories over both land and ocean (Figure 8). The analyzed tropical cloud tops consistently showed ice as the most frequent thermodynamic phase over Sumatra. However, three types of cloud tops were recurrent: thin ice, thick ice, and multilayer. Over Sumatra, thin ice occurs most often before noon, while in the late evening, the proportion of thick ice reaches a maximum during the development of diurnally driven deep clouds. Early morning multilayer clouds dominate during propagation offshore from Sumatra. Frequencies over the ocean are more homogeneous than over land, with the maximum being observed in the morning when the cloud population is located over the adjacent seas of Sumatra. However, the diurnal variation of cloudiness is modified as a response to the enhanced or suppressed convective phases of the MJO. During the MJO-suppressed convective phase, there is a larger number of days without cloud cover owing to the subsidence of the large-scale convective structure over the MC, increasing the relative abundance of the warm clouds (MJO: 6, 7, and 8). In contrast, the enhanced convective phase of the MJO increases the cloud cover over the western MC (MJO: 2, 3, and 4), and a higher proportion of thick ice clouds in the MJO enhanced convective phases, and less diurnal variation in thick ice proportion is observed.

4. Discussion

We have investigated how the DC develops over the western MC based on an intraseasonal analysis of satellite-derived rainfall and RPA. Diurnally driven convection and cloud population features between land, ocean, and coastal regions have been examined over Sumatra. The analysis of deep convective clouds based on the RPA is presented to identify the diurnal and semi-diurnal variations of deep convective clouds, the offshore propagation of the DC of cloud populations and the interaction between Sumatra, Borneo and Java, and the intraseasonal effects over the cloud properties in the western region of the MC and the eastern IO. The DC of the satellite-derived RPA frequency over land and ocean shows an inhomogeneous spatial distribution of cloud populations during the Austral summer DJF between 2016 and 2021 (Figure 3), which is in agreement with previous findings based on satellite-based rainfall by Qian (2008), Kamimera et al. (2012), As-syakur et al. (2019), and Mori et al. (2004). Our findings complement previous studies (As-syakur et al., 2019; Mori et al., 2004; Qian, 2020; Vincent & Lane, 2017) by providing an enhanced description of diurnally driven convection patterns and cloud physical properties over Sumatra with unprecedented fine-scale spatial and temporal detail as well as broad spatial extent.

To answer the first aim of this study, the RPA brings a unique angle compared to a similar analysis based on TRMM data (e.g., Rauniyar et al., 2017; Sakaeda et al., 2020). Over land, the peak diurnal amplitude of rainfall from IMERG (Figure 2) occurs around the time when the frequency of RPA peaks (Figure 3), indicating that the DC is primarily driven by deep convective clouds, consistent with Vincent and Huang (2022) who showed a direct thermodynamic response surface heating on modulating the onset of diurnally initiated rainfall. As shown by the dotted line in Figure 4, the RPA fraction is linked to deep clouds over land. A maximum high RPA fraction was observed over land (Sumatra) through the night and until early morning. The coastal region over the IO (~200 km from the WCS, the salmon line in Figure 4) is highly influenced by the diurnally driven convection propagating off Sumatra with peak time delay associated with the progression of the convective envelope from Sumatra, adding evidence of the importance of land heating processes (Short et al., 2019; Vincent & Lane, 2016) and intraseasonal variability such as MJO (Birch et al., 2016; Peatman et al., 2014). This result also provides observational evidence of the rapid decrease of diurnal signatures from the coastline, adding a coherent description of deep convective clouds over the coastal region. The salmon line in Figure 4 is consistent with a rapid decrease of the water vapor transport within 300 km off the coastline shown in reanalysis data (Ogino et al., 2017) and rainfall patterns (Ogino et al., 2016).

In contrast, over the IO, we hypothesize that the RPA fraction is reduced due to the contribution of stratiform and shallow convective clouds over the ocean to total cloud populations and rainfall, as discussed by Schumacher and Houze (2003) and Sakaeda et al. (2020). The satellite-derived RPA fraction is consistent with previous studies where convective and stratiform rainfall were explored by using TRMM radar data (Schumacher & Houze, 2003), demonstrating that convective rain dominates the total rainfall over the major islands in the MC and the ratio of convective contribution reduces over the IO and some regions of the internal seas of the MC (Hayden et al., 2023; Mori et al., 2004; Renggono et al., 2001; Sakaeda et al., 2020; Vincent & Lane, 2016). An interesting new finding is a semi-diurnal signature over the eastern IO (the solid cyan line in Figure 4), which appears as a combination

of the offshore diurnal cycle of deep convective clouds and the propagating diurnal cycle from the WCS. This feature is entirely different from the phase of the DC propagation from the western mountain ranges of Sumatra and the semi-diurnal signatures of the smaller islands near Sumatra (islands with an area >315 km^2). The semi-diurnal effects can be linked to the remnant of sinusoidal time dependence of the incident solar radiation over the land, which is associated with convergence and divergence, and rainfall patterns over the open ocean and land due to the atmospheric global tide (Christophersen et al., 2020; Dai & Deser, 1999). The semi-diurnal variations over the IO may therefore be explained as a compound effect between the diurnally driven convection propagating off Sumatra and the atmospheric tide. However, that analysis is beyond the scope of this paper. This semi-diurnal signature also appears in Figure 5. Two weak peaks between 01:00–07:00 LST and 13:00–19:00 LST are extended almost horizontally over 300–2,000 km from the WCS, noting that the diurnal variability over the eastern IO also depends on diurnal precipitation and diurnal atmospheric stability according to Fujita et al. (2013). This subtle but important feature could only have been detected using very high spatial, temporal, and spectral resolution data such as that from Himawari-8 AHI.

The second aim of this study was to examine the diurnal and non-local impacts on the development of organized convection. This aim was addressed using the diurnally averaged Hovmöller diagrams of RPA over strategically chosen transects. A detailed description of the propagation of the diurnally driven convection across Sumatra has shown the mean diurnal signatures of clouds populations and their interactions between Sumatra and surrounding islands and the Malay Peninsula during the Austral Summer (Figures 5 and 6). The results of this study indicate that the RPA propagates from the convective initiation regions near the East and West coast of Sumatra, similar to the rainfall patterns from IMERG. Thus, the morning rain can be linked to the coastal activity peaking in the early morning hours, and some cold cloud cores develop offshore Sumatra, peaking in the late morning to noon. However, some regions in Sumatra are controlled by coastal activity (see the Hovmöller diagram Figures 5c and 5d), where inland propagating cloud tops from both coastlines and Bangka-Belitung Islands regions converge over the mountain ranges of Sumatra, showing variations of deep clouds and substructures inland over the central-south region of Sumatra. This also accords with earlier investigations, which showed local rainfall patterns based on TRMM, radar, and satellite measurements by Mori et al. (2004), Sobel et al. (2011, 2013), Kamimera et al. (2012), and As-syakur et al. (2019).

Another important finding was that the mean speed of propagation of the diurnal signatures of the RPA is ∼20 m s^{-1} over the Java Sea. This finding extends the existing knowledge of mechanism of propagation of the diurnally driven convection by providing an explicit sea-ward propagation pattern of deep convection/cloud tops and their interactions between Sumatra, Borneo, and Java at this speed (Figure 6). Our study provides solid evidence of these propagation patterns of deep convection that previous studies presented in isolated cases, implicitly or via rainfall signals (Araki et al., 2006; Mori et al., 2018; Ruppert et al., 2020; Wu, Manabu, & Matsumoto, 2008). These results can be interpreted as the diurnal-phase gravity waves coupled with diurnal mesoscale convective systems in the MC. The inertia gravity waves have been suggested as a mechanism of propagation of the diurnally driven convection by observational and numerical modeling studies (Hassim et al., 2016; Mapes et al., 2003; Ruppert et al., 2020; Short et al., 2019; Vincent & Lane, 2016; Yang & Slingo, 2001), where thermal instability acts as forcing at the lower troposphere. Thermal disturbances propagate by inertia-gravity waves triggered by diurnally oscillating heating and the effects of mixed layers over the adjacent regions propagating away from the regions of afternoon convective response. Instability resulting from the vertical structure of these disturbances has been suggested to generate nocturnal cloud populations along the coastlines of Sumatra, Java, and Borneo (Figure 6a) and the Java Sea (Figure 6b) (Mori et al., 2004; Ruppert et al., 2019; Short et al., 2019; Vincent & Lane, 2016). That these minor perturbations in instability are enough to trigger the cold cloud tops associated with deep convection.

Our results also reflect the influence of the large-scale circulation over the oceans to the south of the equator. The daily variations of the diurnal cloud tops and the westward propagation distance from the WCS are driven by background thermodynamics, the seasonal position and structure of the ITCZ, the Asia-Australian monsoon, and semi-permanent circulations over the southern IO (As-syakur et al., 2019; Murakami & Matsumoto, 1994; Qian, 2020; Sakurai et al., 2005). These results reflect those of Murakami and Matsumoto (1994), Hamada et al. (2002), Sakurai et al. (2005), and Qian (2020) who also found a different convective regime in both hemispheres (over land Sumatra): The northern hemisphere region of Sumatra presents a semi-dry season during Austral Summer. In contrast, the southern hemisphere region of Sumatra shows a wet season. The cloud environment and its DC are fundamentally governed by the scale interaction between the mean background state, the

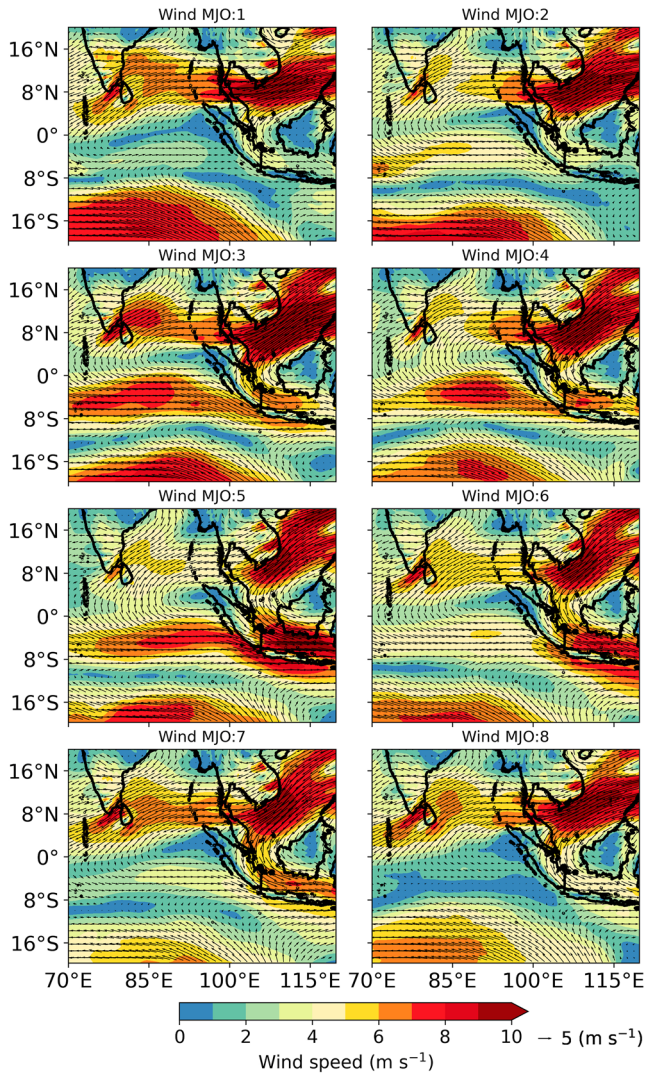

Figure 9. Mean 925–850 hPa wind vectors and wind speed (shaded, m s^{-1}) over the Indian Ocean and the Maritime Continent from ERA5 for Austral Summer (2016–2021) by MJO phases.

intraseasonal scale, and the mesoscale flows, none of which tells the whole story in isolation.

To expand these arguments, we show the 925–850 hPa wind vectors and the vertically integrated moisture divergence, in addition averaged by MJO phase in Figures 9 and 10, respectively. In southern Sumatra and surrounding areas, the constant contribution of moist air on the WCS induces the development of storms in southwestern Sumatra with a diurnal signature (As-syakur et al., 2019; Kerns & Chen, 2016; Mori et al., 2004; Qian, 2020; Sakurai et al., 2005; Short et al., 2019). This is the case for all MJO phases, except for Phase 8, despite the strength of the onshore flow varying with the easterly or westerly anomalies of the MJO. However, the background moisture availability modulates the VIMD associated with this onshore flow. The diurnal rainfall patterns on a local scale are driven by complex cross-equatorial interactions (Figure 10), background wind flows through the western ridges of the island, which have an average height of 2,000 m, and the contribution of the DC from the surrounding islands of Sumatra (Figure 1). For example, note the variation in wind direction in southern Sumatra, which alters the onshore and topographic aspects of the flow. Looking at local signatures, the Strait of Malacca (Figures 5a and 5b) and the Java Sea (Figure 6b) show combined patterns of the DC of the RPA between Sumatra, Java, and Borneo. Additionally, wind analyses are consistent with local wind convergence of the DC (early morning land breeze) from Sumatra and Malay Peninsula and its intraseasonal variations demonstrated by Virts et al. (2013) and Qian (2020). The mean diurnal propagations observed are associated with large-scale lower tropospheric wind forcing (Qian, 2008; Short et al., 2019; Wang & Sobel, 2017; Yanase et al., 2017), which is highly influenced by the intraseasonal variability of wind (Figure 9) and moisture flux convergence (Figure 10) during the MJO enhanced and suppressed convective phases and equatorial waves.

The third aim of this study is related to the spatiotemporal distribution of cloud top types. Composites of mean cloud top type over land and ocean Sumatra in Figure 8 during the MJO enhanced and suppressed convective phases showed the three most frequent categories: thick ice, thin ice, and multilayer, with the largest diurnal variation found in the thick ice, which peaks in the mid-late afternoon. This study found that the DC of ice in the tropics is characterized by deep convective systems with a large amount of thin and thick ice in the upper tropopause. Dion et al. (2019, 2021) showed the primary role of deep convective clouds in ice distribution in different levels of the troposphere at a diurnal scale in the MC and also demonstrated a strong correlation between the maximum and minimum amount and rainfall production during the different stages of the DC. Cloudiness increases across the domain as the region of enhanced convective phase approaches from the west. Then cloud amount decreases as the region of the enhanced convective phase of MJO shifts eastward into the western Pacific. However, the new satellite-derived patterns of MJO cloud physical properties are visually complex, and the spatial patterns were examined in more detail in animations of normalized composites of cloud top type (Thin ice: Movie S2, Thick ice: Movie S3, and Multilayer: Movie S4) from Himawari-8 AHI. Composites of thick ice show clouds with high emissivity and IR optical depths >2, while thin ice includes clouds with IR optical depths ≤2, and multilayer includes high and low clouds (liquid + ice clouds). Extensive cloudiness is observed over Sumatra and the interior seas of the MC during all MJO phases. However, thick ice is linked to the signature of the diurnally driven convection for its physical characteristics during the afternoon when the deep convective events are more locally controlled by land (Dion et al., 2019, 2021). These patterns could also mean that the propagation distance tends to be reduced offshore Sumatra. However, intra-seasonal modes of variability modify the atmospheric conditions at the local scale, affecting the structure of the land-sea-breeze system (Lopez-Bravo et al., 2023; Mori et al., 2004; Sakaeda et al., 2020; Seiki et al., 2021; Short et al., 2019; Vincent & Lane, 2016). The DC

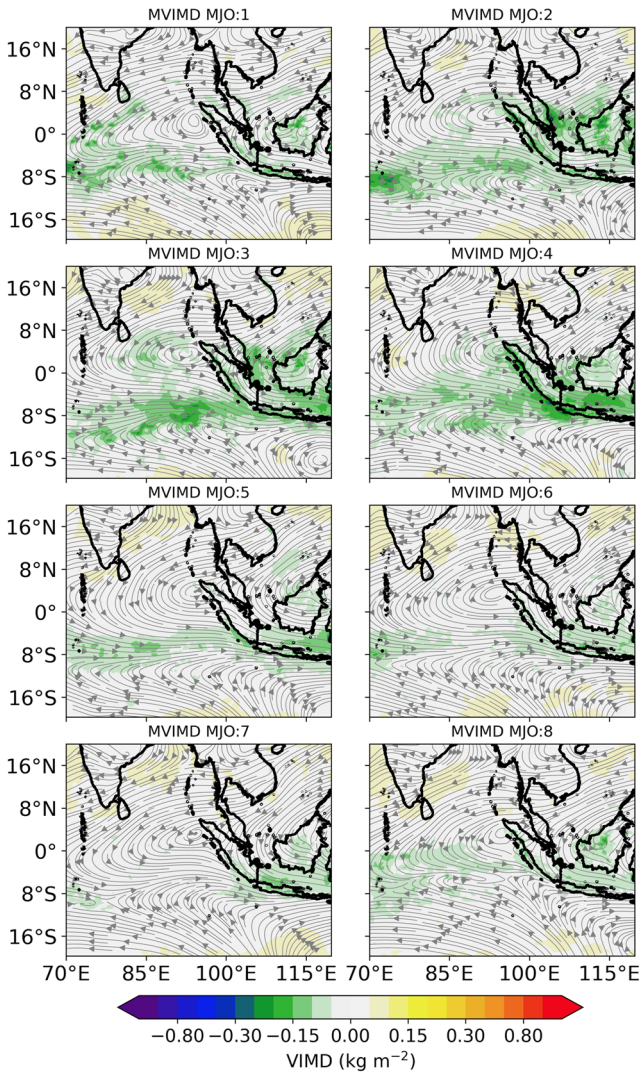

Figure 10. Composite of vertically integrated moisture divergence from the surface of the Earth to the top of the atmosphere (VIMD, kg m^{-2}) and 925–850 hPa streamlines from ERA5 for Austral summer (2016–2021) by MJO phases.

over the IO strengthens during the MJO-enhanced convective phases. Similar signatures are observed in thin ice and multilayer categories, but the spatial distribution can be a proxy for the non-convective contributions of the cloud populations. This modulation has been suggested to be mechanically forced by large-scale lower tropospheric background wind flow (Qian, 2008; Wang & Sobel, 2017; Yanase et al., 2017) as shown in Figure 9, but the importance of wind anomalies, moisture distribution, and vertically integrated moisture convergence (Figure 10) also play an important role on the propagation of the mesoscale convective systems over Sumatra (Birch et al., 2016; Lu et al., 2019; Rauniyar et al., 2017; Sakaeda et al., 2020; Seiki et al., 2021; Vincent & Lane, 2016). The distribution of hydrometer species has been shown to be poorly represented in modeling systems on various scales. These results are important to model evaluations and development in this area.

5. Conclusions

Over Sumatra and surrounding islands, the land- and sea-breeze systems and background wind flow regimes forced by the diurnal heating are the primary mechanisms for the strong lifting needed to initiate a deep tropical convective environment. This work has explored an alternative to investigating the diurnally driven convection over the land in Sumatra, the internal seas of the western Maritime Continent (MC), and the equatorial eastern Indian Ocean. Our results based on Rainfall Potential Areas (RPA) allowed the identification of the diurnal and semi-diurnal variations of deep convective clouds over the Indian Ocean (IO, distance between 200 and 950 km), the sea-ward propagation of the diurnally driven convection and the interaction between diurnal cycles (DC)s of Sumatra, Borneo, and Java at unprecedented spatial resolution. Additionally, the findings of this work contribute the existing knowledge of cloud variability of the DC by MJO phases over the western region of the MC for Austral Summer. This work used state-of-art satellite imagery, including thermal and water vapor infrared spectral bands, cloud properties from Himawari-8 AHI, and satellite-based rainfall estimates from IMERG (December-January-February, 2016–2021). The analysis showed:

1. That there is a transition from the land mean diurnal cycle to the open-ocean mean diurnal cycle at 220–450 km off the SW coast of Sumatra, leading to a semi-diurnal cycle in the transition region driven by the DC of Sumatra, and radiative effects over the IO.
2. The effects of synchronized diurnal cycles between Sumatra, Borneo, and Java, including interactions of inertia-gravity wave type propagation from adjacent coasts;
3. That there are deep convective cloud-top latitudinal variations over the IO.
4. That there are differences in the average CTH over RPAs at the diurnal maximum depending on MJO phase;
5. That the diurnal variability of thick ice clouds varies between the MJO-enhanced and suppressed convective phases.

The dynamical and thermodynamical setting for these observations was examined through seasonal analysis of moisture convergence and background wind in the lower troposphere.

Our investigation contributes to existing knowledge of local cloud variability over land. Local variations are characterized by features of cloud population propagation from the coastline to the inland region during the day and cloudiness propagating toward the coast at night. However, the influence of the geometry of Sumatra on intercoastal activity is most evident in southern Sumatra, where the distance between the coasts of Sumatra is approximately 300 km, nearly double that of North Sumatra. Here, the analysis of RPA at high spatial resolution sheds new insights on the convective diurnal signatures by detecting inland-propagating substructures of cloud populations that have not been possible to characterize in previous studies (As-syakur et al., 2019;

Mori et al., 2018; Ruppert et al., 2020). The evidence from this study provides for the first time an explicit signature of the sea-ward propagation of the DC and its interactions between Sumatra, Java, and Borneo, consistent with implicit descriptions in Araki et al. (2006), Wu, Manabu, and Matsumoto (2008), and Mori et al. (2018).

This is the first study that uses high-resolution geostationary satellite-derived cloud properties to explore the influence of the MJO over the diurnal cycle over Sumatra. A comprehensive analysis of satellite-derived cloud properties from geostationary data and CSPP-Geo GEOCAT showed that most of the convective clouds develop along the southwest coast of Sumatra between 06:00 and 13:00 and 19:00 LST, with an average range of the CTH between 11.5 and 12.5 km based on Himawari-8 AHI. The results show that the mean CTH is systematically higher over southern Sumatra, showing a similar trend across all the MJO phases analyzed. Before this study, evidence of the DC was based on the distribution of rainfall, IR analysis using a single band, or radar data. The results also showed that the CTH is on average higher, and the cold cloud area larger, in the MJO-enhanced convection phases and contains more thick ice clouds. These effects are linked to the diurnally driven convection over the mountain ranges of Sumatra, the eastern Indian Ocean, and the interior seas of the MC.

The RPA and cloud top type variability have revealed evidence of the effects of convective processes on the diurnal cycle of ice and water vapor distribution in the troposphere. Like most aspects of the diurnal variations in the MC, these diurnal variations are also driven by the MJO-enhanced and suppressed convective phases, where cloudiness tends to amplify the climatological-mean DC in some areas and decrease it in others.

It should be noted that the approaches in this analysis have some limitations. For example, the cold cloud cores in the transition zone between the middle and upper troposphere are not detected efficiently by the RPA approach. Additionally, the proportion of stratiform clouds cannot be estimated due to the algorithm, and the vertical structure is not resolved, which is dictated by the physics of the measurement in geostationary satellites, and this affects the estimation over the ocean. Moreover, the RPA offers a flag for the existence of rainfall from deep convective clouds, which means that, by definition, the intensity and accumulated rainfall amounts are not considered here. Despite these shortcomings, the use of RPA, rather than all rainfall (e.g., as estimated by IMERG) means that any detected signals will come from deep convection and cold cloud tops, thus indicating a relatively strong response to propagating disturbances.

Finally, The findings in this study build on existing knowledge about the diurnal cycle over Sumatra by filling a gap in understanding the deep convective local signatures and cloud properties, including evidence of the semi-diurnal frequency of deep convective clouds over the eastern IO and the multi-scale spatiotemporal variation of thick ice clouds over Sumatra. There are several broader implications of this work:

1. This work shows the multi-scale sensitivity of RPA to both background dynamical and thermodynamical conditions. This is critical for extreme weather predictions and climate projections in the region, bearing in mind that the RPA areas relate to heavy convective rainfall that is implicitly linked with the potential for heavy rainfall and flash flooding.
2. The subtle transition between land and ocean diurnal cycles expands our knowledge about offshore propagating convective systems but raises questions about the width and temporal consistency of the transition zone.
3. The distribution of hydrometeor species is an ongoing challenge in all atmospheric models. The approaches shown here provide an avenue for model evaluation and development, albeit only considering the cloud top types. The importance of the increase in thick ice clouds and increase in average CTH over the RPAs during the MJO convectively enhanced phases, both in terms of inter-scale impacts and rainfall extremes is not fully understood at this stage but should be evaluated through modeling and radar data sets.

Data Availability Statement

The Himawari-8 GeoCat 1.0.3 Australian Domain Collections level 1 and 2 were used to explore the diurnally forced convection over Sumatra. Data sets are available at NCI National Research Data Collection, Australia via https://doi.org/10.25914/60096221a8f7a (level 1) and https://doi.org/10.25914/60096228c7ec0 (level 2) with Creative Commons Attributions 4.0 International license. Version 1.0.3 of the CSPP-Geo GEOCAT was provided by the CSPP Geo project (CIMSS—UW-Madison). URL: http://cimss.ssec.wisc.edu/csppgeo/geocat.html.

Acknowledgments
This work was funded by the Melbourne Research Scholarship and the Australian Research Council (ARC) Discovery Project DP190100786 for C. Lopez-Bravo and the ARC Centre of Excellence for Climate Extremes CE170100023 for C. Vincent, Y. Huang, and T. P. Lane. The production of derived-satellite data from Himawari-8 AHI for this research was undertaken on the NCI National Facility in Canberra, Australia, supported by the Australian Commonwealth Government. The authors wish to thank the three reviewers for their insightful feedback. The authors wish to thank the JMA Meteorological Satellite Center, The Bureau of Meteorology, Australia, and the CSPP Geo project (CIMSS—UW-Madison). Thanks also to Paola Petrelli of the University of Tasmania and Kelsey Druken of the Australian National University for assistance during the data set publication process.

References

Araki, R., Yamanaka, M. D., Murata, F., Hashiguchi, H., Oku, Y., Sribimawati, T., et al. (2006). Seasonal and interannual variations of diurnal cycles of wind and cloud activity observed at Serpong, West Jawa, Indonesia. *Journal of the Meteorological Society of Japan. Series II*, *84A*, 171–194. https://doi.org/10.2151/jmsj.84A.171

As-syakur, A. R., Imaoka, K., Ogawara, K., Yamanaka, M. D., Tanaka, T., Kashino, Y., et al. (2019). Analysis of spatial and seasonal differences in the diurnal rainfall cycle over Sumatera revealed by 17-year TRMM 3B42 dataset. *Scientific Online Letters on the Atmosphere*, *15*(0), 216–221. https://doi.org/10.2151/sola.2019-039

Bergemann, M., & Jakob, C. (2016). How important is tropospheric humidity for coastal rainfall in the tropics? *Geophysical Research Letters*, *43*(11), 5860–5868. https://doi.org/10.1002/2016GL069255

Beucher, S. (1979). Use of watersheds in contour detection. In *Proceedings of the international workshop on image processing*.

Birch, C. E., Webster, S., Peatman, S. C., Parker, D. J., Matthews, A. J., Li, Y., & Hassim, M. E. E. (2016). Scale interactions between the MJO and the western Maritime Continent. *Journal of Climate*, *29*(7), 2471–2492. https://doi.org/10.1175/JCLI-D-15-0557.1

Christophersen, J. A., Foltz, G. R., & Perez, R. C. (2020). Surface expressions of atmospheric thermal tides in the tropical Atlantic and their impact on open-ocean precipitation. *Journal of Geophysical Research: Atmospheres*, *125*(22), e2019JD031997. https://doi.org/10.1029/2019JD031997

Dai, A., & Deser, C. (1999). Diurnal and semidiurnal variation in global surface wind and divergence fields. *Journal of Geophysical Research*, *104*(D24), 31109–31125. https://doi.org/10.1029/1999JD900927

Da Silva, N. A., Webber, B. G. M., Matthews, A. J., Feist, M. M., Stein, T. H. M., Holloway, C. E., & Abdullah, M. F. A. B. (2021). Validation of GPM IMERG extreme precipitation in the Maritime Continent by station and radar data. *Earth and Space Science*, *8*(7), e2021EA001738. https://doi.org/10.1029/2021EA001738

Dion, I.-A., Dallet, C., Ricaud, P., Carminati, F., Dauhut, T., & Haynes, P. (2021). Ice injected into the tropopause by deep convection—Part 2: Over the Maritime Continent. *Atmospheric Chemistry and Physics*, *21*(3), 2191–2210. https://doi.org/10.5194/acp-21-2191-2021

Dion, I.-A., Ricaud, P., Haynes, P., Carminati, F., & Dauhut, T. (2019). Ice injected into the tropopause by deep convection—Part 1: In the austral convective tropics. *Atmospheric Chemistry and Physics*, *19*(9), 6459–6479. https://doi.org/10.5194/acp-19-6459-2019

Fujita, M., Kimura, F., & Yoshizaki, M. (2010). Morning precipitation peak over the Strait of Malacca under a calm condition. *Monthly Weather Review*, *138*(4), 1474–1486. https://doi.org/10.1175/2009MWR3068.1

Fujita, M., Takahashi, H. G., & Hara, M. (2013). Diurnal cycle of precipitation over the eastern Indian Ocean off Sumatra Island during different phases of Indian Ocean Dipole. *Atmospheric Science Letters*, *14*(3), 153–159. https://doi.org/10.1002/asl2.432

Hamada, J.-I., Yamanaka, M. D., Matsumoto, J., Fukao, S., Winarso, P. A., & Sribimawati, T. (2002). Spatial and temporal variations of the rainy season over Indonesia and their link to ENSO. *Journal of the Meteorological Society of Japan. Series II*, *80*(2), 285–310. https://doi.org/10.2151/jmsj.80.285

Hamada, J.-I., Yamanaka, M. D., Mori, S., Tauhid, Y. I., & Sribimawati, T. (2008). Differences of rainfall characteristics between coastal and interior areas of central western Sumatera, Indonesia. *Journal of the Meteorological Society of Japan. Series II*, *86*(5), 593–611. https://doi.org/10.2151/jmsj.86.593

Hassim, M. E. E., & Lane, T. P. (2010). A model study on the influence of overshooting convection on TTL water vapour. *Atmospheric Chemistry and Physics*, *10*(20), 9833–9849. https://doi.org/10.5194/acp-10-9833-2010

Hassim, M. E. E., Lane, T. P., & Grabowski, W. W. (2016). The diurnal cycle of rainfall over New Guinea in convection-permitting WRF simulations. *Atmospheric Chemistry and Physics*, *16*(1), 161–175. https://doi.org/10.5194/acp-16-161-2016

Hayden, L. J. M., Tan, J., Bolvin, D. T., & Huffman, G. J. (2023). Variations in the diurnal cycle of precipitation and its changes with distance from shore over two contrasting regions as observed by IMERG, ERA5, and Spaceborne Ku Radar. *Journal of Hydrometeorology*, *24*(4), 675–689. https://doi.org/10.1175/JHM-D-22-0154.1

Heidinger, A. K., Pavolonis, M. J., Calvert, C., Hoffman, J., Nebuda, S., Straka, W., et al. (2020). Chapter 6—ABI cloud products from the GOES-R series. In S. J. Goodman, T. J. Schmit, J. Daniels, & R. J. Redmon (Eds.), *The GOES-R series* (pp. 43–62). Elsevier. https://doi.org/10.1016/B978-0-12-814327-8.00006-8

Heikenfeld, M., Marinescu, P., Christensen, M., Watson-Parris, D., Senf, F., Heever, S., & Stier, P. (2019). tobac v1.0: Towards a flexible framework for tracking and analysis of clouds in diverse datasets. *Geoscientific Model Development Discussions*, 1–31. https://doi.org/10.5194/gmd-2019-105

Huang, Y., Siems, S., Manton, M., Protat, A., Majewski, L., & Nguyen, H. (2019). Evaluating Himawari-8 cloud products using Shipborne and CALIPSO observations: Cloud-top height and cloud-top temperature. *Journal of Atmospheric and Oceanic Technology*, *36*(12), 2327–2347. https://doi.org/10.1175/JTECH-D-18-0231.1

Huffman, G., Bolvin, D., Braithwaite, D., Hsu, K., Joyce, R., Kidd, C., et al. (2019). NASA global precipitation measurement (GPM) integrated multi-satellite retrievals for GPM (IMERG). In *Algorithm theoretical basis document (ATBD) version 06*. National Aeronautics and Space Administration (NASA).

Huffman, G., Stocker, E., Bolvin, D., Nelkin, E., & Tan, J. (2019). *GPM IMERG final precipitation L3 half Ho@urly 0.1 degree × 0.1 degree V06, Greenbelt, MD, Goddard Earth sciences data and information services center (GES DISC)*. National Aeronautics and Space Administration (NASA).

Huffman, G. J., Bolvin, D. T., Braithwaite, D., Hsu, K.-L., Joyce, R. J., Kidd, C., et al. (2020). Integrated multi-satellite retrievals for the global precipitation measurement (GPM) mission (IMERG). In V. Levizzani, C. Kidd, D. B. Kirschbaum, C. D. Kummerow, K. Nakamura, & F. J. Turk (Eds.), *Satellite precipitation measurement: Volume 1* (pp. 343–353). Springer International Publishing. https://doi.org/10.1007/978-3-030-24568-9_19

JMA. (2015). *Users' guide to imagery with heavy rainfall potential areas*. (Tech. Rep.). Japanese Meteorological Agency.

Kamimera, H., Mori, S., Yamanaka, M. D., & Syamsudin, F. (2012). Modulation of diurnal rainfall cycle by the Madden-Julian Oscillation based on one-year continuous observations with a meteorological radar in west Sumatera. *Scientific Online Letters on the Atmosphere*, *8*(0), 111–114. https://doi.org/10.2151/sola.2012-028

Kerns, B. W., & Chen, S. S. (2016). Large-scale precipitation tracking and the MJO over the Maritime Continent and Indo-Pacific warm pool. *Journal of Geophysical Research: Atmospheres*, *121*(15), 8755–8776. https://doi.org/10.1002/2015JD024661

Kikuchi, K., & Wang, B. (2008). Diurnal precipitation regimes in the global tropics. *Journal of Climate*, *21*(11), 2680–2696. https://doi.org/10.1175/2007JCLI2051.1

Lopez-Bravo, C., Vincent, C. L., & Huang, Y. (2021a). *Himawari-8 GeoCat 1.0.3 Australian domain level 1 v1.0*. NCI National Research Data Collection. https://doi.org/10.25914/60096221a8f7a

Lopez-Bravo, C., Vincent, C. L., & Huang, Y. (2021b). *Himawari-8 GeoCat 1.0.3 Australian domain level 2 v1.0*. NCI National Research Data Collection. https://doi.org/10.25914/60096228c7ec0

Lopez-Bravo, C., Vincent, C. L., Huang, Y., & Lane, T. P. (2023). A case study of a West Sumatra squall line using satellite observations. *Monthly Weather Review*, *151*(2), 523–543. https://doi.org/10.1175/MWR-D-21-0194.1

Love, B. S., Matthews, A. J., & Lister, G. M. S. (2011). The diurnal cycle of precipitation over the Maritime Continent in a high-resolution atmospheric model. *Quarterly Journal of the Royal Meteorological Society*, *137*(657), 934–947. https://doi.org/10.1002/qj.809

Lu, J., Li, T., & Wang, L. (2019). Precipitation diurnal cycle over the Maritime Continent modulated by the MJO. *Climate Dynamics*, *53*(9), 6489–6501. https://doi.org/10.1007/s00382-019-04941-8

Mapes, B. E., Warner, T. T., & Xu, M. (2003). Diurnal patterns of rainfall in northwestern South America. Part III: Diurnal gravity waves and nocturnal convection offshore. *Monthly Weather Review*, *131*(5), 830–844. https://doi.org/10.1175/1520-0493(2003)131⟨0830:DPORIN⟩2.0.CO;2

Mori, S., Hamada, J.-I., Hattori, M., Wu, P.-M., Katsumata, M., Endo, N., et al. (2018). Meridional march of diurnal rainfall over Jakarta, Indonesia, observed with a C-band Doppler radar: An overview of the HARIMAU2010 campaign. *Progress in Earth and Planetary Science*, *5*, 1–23. https://doi.org/10.1186/s40645-018-0202-9

Mori, S., Jun-Ichi, H., Tauhid, Y. I., Yamanaka, M. D., Okamoto, N., Murata, F., et al. (2004). Diurnal land-sea rainfall peak migration over Sumatera Island, Indonesian Maritime Continent, observed by TRMM satellite and intensive rawinsonde soundings. *Monthly Weather Review*, *132*(8), 2021–2039. https://doi.org/10.1175/1520-0493(2004)132⟨2021:DLRPMO⟩2.0.CO;2

Murakami, T., & Matsumoto, J. (1994). Summer monsoon over the Asian continent and western North Pacific. *Journal of the Meteorological Society of Japan. Series II*, *72*(5), 719–745. https://doi.org/10.2151/jmsj1965.72.5_719

Navarro, A., García-Ortega, E., Merino, A., Sánchez, J. L., Kummerow, C., & Tapiador, F. J. (2019). Assessment of IMERG precipitation estimates over Europe. *Remote Sensing*, *11*(21), 2470. https://doi.org/10.3390/rs11212470

Neale, R., & Slingo, J. (2003). The Maritime Continent and its role in the global climate: A GCM study. *Journal of Climate*, *16*(5), 834–848. https://doi.org/10.1175/1520-0442(2003)016⟨0834:TMCAIR⟩2.0.CO;2

Nesbitt, S. W., & Zipser, E. J. (2003). The diurnal cycle of rainfall and convective intensity according to three years of TRMM measurements. *Journal of Climate*, *16*(10), 1456–1475. https://doi.org/10.1175/1520-0442(2003)016⟨1456:TDCORA⟩2.0.CO;2

Nieuwolt, S. (1968). Diurnal rainfall variation in Malaya. *Annals of the Association of American Geographers*, *58*(2), 313–326. https://doi.org/10.1111/j.1467-8306.1968.tb00646.x

Ogino, S.-Y., Yamanaka, M. D., Mori, S., & Matsumoto, J. (2016). How much is the precipitation amount over the tropical coastal region? *Journal of Climate*, *29*(3), 1231–1236. https://doi.org/10.1175/JCLI-D-15-0484.1

Ogino, S.-Y., Yamanaka, M. D., Mori, S., & Matsumoto, J. (2017). Tropical coastal dehydrator in global atmospheric water circulation. *Geophysical Research Letters*, *44*(22), 11636–11643. https://doi.org/10.1002/2017GL075760

Oh, J.-H., Kim, K.-Y., & Lim, G.-H. (2012). Impact of MJO on the diurnal cycle of rainfall over the western Maritime Continent in the austral summer. *Climate Dynamics*, *38*(5), 1167–1180. https://doi.org/10.1007/s00382-011-1237-4

Pavolonis, M. (2010). *GOES-R advanced baseline imager (ABI) algorithm theoretical basis document for cloud type and cloud phase*. NOAA NESDIS Center for Satellite Applications and Research.

Peatman, S. C., Matthews, A. J., & Stevens, D. P. (2014). Propagation of the Madden–Julian Oscillation through the Maritime Continent and scale interaction with the diurnal cycle of precipitation. *Quarterly Journal of the Royal Meteorological Society*, *140*(680), 814–825. https://doi.org/10.1002/qj.2161

Peatman, S. C., Schwendike, J., Birch, C. E., Marsham, J. H., Matthews, A. J., & Yang, G.-Y. (2021). A local-to-large scale view of Maritime Continent rainfall: Control by ENSO, MJO, and equatorial waves. *Journal of Climate*, *34*(22), 8933–8953. https://doi.org/10.1175/JCLI-D-21-0263.1

Qian, J.-H. (2008). Why precipitation is mostly concentrated over islands in the Maritime Continent. *Journal of the Atmospheric Sciences*, *65*(4), 1428–1441. https://doi.org/10.1175/2007JAS2422.1

Qian, J.-H. (2020). Multi-scale climate processes and rainfall variability in Sumatra and Malay Peninsula associated with ENSO in boreal fall and winter. *International Journal of Climatology*, *40*(9), 4171–4188. https://doi.org/10.1002/joc.6450

Rauniyar, S. P., Protat, A., & KanaMori, H. (2017). Uncertainties in TRMM-Era multisatellite-based tropical rainfall estimates over the Maritime Continent. *Earth and Space Science*, *4*(5), 275–302. https://doi.org/10.1002/2017EA000279

Rauniyar, S. P., & Walsh, K. J. E. (2011). Scale interaction of the diurnal cycle of rainfall over the Maritime Continent and Australia: Influence of the MJO. *Journal of Climate*, *24*(2), 325–348. https://doi.org/10.1175/2010JCLI3673.1

Renggono, F., Hashiguchi, H., Fukao, S., Yamanaka, M. D., Ogino, S.-Y., Okamoto, N., et al. (2001). Precipitating clouds observed by 1.3-GHz boundary layer radars in equatorial Indonesia. *Annals of Geophysics*, *19*(8), 889–897. https://doi.org/10.5194/angeo-19-889-2001

Ruppert, J., James, H., & Chen, X. (2020). Island rainfall enhancement in the Maritime Continent. *Geophysical Research Letters*, *47*(5), e2019GL086545. https://doi.org/10.1029/2019GL086545

Ruppert, J., James, H., & Zhang, F. (2019). Diurnal forcing and phase locking of gravity waves in the Maritime Continent. *Journal of the Atmospheric Sciences*, *76*(9), 2815–2835. https://doi.org/10.1175/JAS-D-19-0061.1

Sakaeda, N., Kiladis, G., & Dias, J. (2017). The diurnal cycle of tropical cloudiness and rainfall associated with the Madden–Julian Oscillation. *Journal of Climate*, *30*(11), 3999–4020. https://doi.org/10.1175/JCLI-D-16-0788.1

Sakaeda, N., Kiladis, G., & Dias, J. (2020). The diurnal cycle of rainfall and the convectively coupled equatorial waves over the Maritime Continent. *Journal of Climate*, *33*(8), 3307–3331. https://doi.org/10.1175/JCLI-D-19-0043.1

Sakurai, N., Kawashima, M., Fujiyoshi, Y., Hashiguchi, H., Shimomai, T., Mori, S., et al. (2009). Internal structures of migratory cloud systems with diurnal cycle over Sumatera island during CPEA-I campaign. *Journal of the Meteorological Society of Japan. Series II*, *87*(1), 157–170. https://doi.org/10.2151/jmsj.87.157

Sakurai, N., Murata, F., Yamanaka, M. D., Mori, S., Hamada, J.-I., Hashiguchi, H., et al. (2005). Diurnal cycle of cloud system migration over Sumatera Island. *Journal of the Meteorological Society of Japan. Series II*, *83*(5), 835–850. https://doi.org/10.2151/jmsj.83.835

Schumacher, C., & Houze, R. A. (2003). Stratiform rain in the tropics as seen by the TRMM precipitation radar. *Journal of Climate*, *16*(11), 1739–1756. https://doi.org/10.1175/1520-0442(2003)016⟨1739:SRITTA⟩2.0.CO;2

Scott, J. R. (1956). The zonal wind in the upper troposphere and weather at Singapore. *Quarterly Journal of the Royal Meteorological Society*, *82*(353), 340–341. https://doi.org/10.1002/qj.49708235310

Seiki, A., Yokoi, S., & Katsumata, M. (2021). The impact of diurnal precipitation over Sumatra Island, Indonesia, on synoptic disturbances and its relation to the Madden-Julian Oscillation. *Journal of the Meteorological Society of Japan. Series II*, *99*(1), 113–137. https://doi.org/10.2151/jmsj.2021-007

Short, E., Vincent, C. L., & Lane, T. P. (2019). Diurnal cycle of surface winds in the Maritime Continent observed through satellite scatterometry. *Monthly Weather Review*, *147*(6), 2023–2044. https://doi.org/10.1175/MWR-D-18-0433.1

Sobel, A. H., Burleyson, C. D., & Yuter, S. E. (2011). Rain on small tropical islands. *Journal of Geophysical Research*, *116*(D8), D08102. https://doi.org/10.1029/2010JD014695

Sobel, A. H., Burleyson, C. D., Yuter, S. E., & Biasutti, M. (2013). Correction to "rain on small tropical islands". *Journal of Geophysical Research: Atmospheres*, *118*(5), 2301–2302. https://doi.org/10.1002/jgrd.50205

Sungmin, O., & Kirstetter, P.-E. (2018). Evaluation of diurnal variation of GPM IMERG-derived summer precipitation over the contiguous US using MRMS data. *Quarterly Journal of the Royal Meteorological Society*, *144*(S1), 270–281. https://doi.org/10.1002/qj.3218

Takayabu, Y. N. (1994). Large-scale cloud disturbances associated with equatorial waves. *Journal of the Meteorological Society of Japan. Series II*, *72*(3), 433–449. https://doi.org/10.2151/jmsj1965.72.3_433

Tan, J., Huffman, G. J., Bolvin, D. T., & Nelkin, E. J. (2019). Diurnal cycle of IMERG V06 precipitation. *Geophysical Research Letters*, *46*(22), 13584–13592. https://doi.org/10.1029/2019GL085395

Tapiador, F. J., Navarro, A., García-Ortega, E., Merino, A., Sánchez, J. L., Marcos, C., & Kummerow, C. (2020). The contribution of rain gauges in the calibration of the IMERG product: Results from the first validation over Spain. *Journal of Hydrometeorology*, *21*(2), 161–182. https://doi.org/10.1175/JHM-D-19-0116.1

Teo, C.-K., Koh, T.-Y., Lo, J. C.-F., & Bhatt, B. C. (2011). Principal component analysis of observed and modeled diurnal rainfall in the Maritime Continent. *Journal of Climate*, *24*(17), 4662–4675. https://doi.org/10.1175/2011JCLI4047.1

Tulich, S. N., & Mapes, B. E. (2008). Multiscale convective wave disturbances in the tropics: Insights from a two-dimensional cloud-resolving model. *Journal of the Atmospheric Sciences*, *65*(1), 140–155. https://doi.org/10.1175/2007JAS2353.1

Vincent, C. L., & Huang, Y. (2022). Meso- and microscale response to variation in cloudiness at three forested sites in the Maritime Continent. *Quarterly Journal of the Royal Meteorological Society*, *148*(742), 418–433. https://doi.org/10.1002/qj.4212

Vincent, C. L., & Lane, T. P. (2016). Evolution of the diurnal precipitation cycle with the passage of a Madden-Julian Oscillation event through the Maritime Continent. *Monthly Weather Review*, *144*(5), 1983–2005. https://doi.org/10.1175/MWR-D-15-0326.1

Vincent, C. L., & Lane, T. P. (2017). A 10-year austral summer climatology of observed and modeled intraseasonal, mesoscale, and diurnal variations over the Maritime Continent. *Journal of Climate*, *30*(10), 3807–3828. https://doi.org/10.1175/JCLI-D-16-0688.1

Virts, K. S., Thornton, J. A., Wallace, J. M., Hutchins, M. L., Holzworth, R. H., & Jacobson, A. R. (2011). Daily and intraseasonal relationships between lightning and NO_2 over the Maritime Continent. *Geophysical Research Letters*, *38*(19). https://doi.org/10.1029/2011GL048578

Virts, K. S., Wallace, J. M., Hutchins, M. L., & Holzworth, R. H. (2013). Diurnal lightning variability over the Maritime Continent: Impact of low-level winds, cloudiness, and the MJO. *Journal of the Atmospheric Sciences*, *70*(10), 3128–3146. https://doi.org/10.1175/JAS-D-13-021.1

Wang, S., & Sobel, A. H. (2017). Factors controlling rain on small tropical islands: Diurnal cycle, large-scale wind speed, and topography. *Journal of the Atmospheric Sciences*, *74*(11), 3515–3532. https://doi.org/10.1175/JAS-D-16-0344.1

Watters, D., Battaglia, A., & Allan, R. P. (2021). The diurnal cycle of precipitation according to multiple decades of global satellite observations, three CMIP6 models, and the ECMWF reanalysis. *Journal of Climate*, *34*(12), 5063–5080. https://doi.org/10.1175/JCLI-D-20-0966.1

Wheeler, M. C., & Hendon, H. H. (2004). An all-season real-time multivariate MJO index: Development of an index for monitoring and prediction. *Monthly Weather Review*, *132*(8), 1917–1932. https://doi.org/10.1175/1520-0493(2004)132⟨1917:AARMMI⟩2.0.CO;2

Worku, L. Y., Mekonnen, A., & Schreck, C. J., III. (2019). Diurnal cycle of rainfall and convection over the Maritime Continent using TRMM and ISCCP. *International Journal of Climatology*, *39*(13), 5191–5200. https://doi.org/10.1002/joc.6121

Wu, P., Manabu, D. Y., & Matsumoto, J. (2008). The Formation of nocturnal rainfall offshore from convection over western Kalimantan (Borneo) island. *Journal of the Meteorological Society of Japan. Series II*, *86A*, 187–203. https://doi.org/10.2151/jmsj.86A.187

Wu, P., Mori, S., Hamada, J.-I., Yamanaka, M. D., Matsumoto, J., & Kimura, F. (2008). Diurnal variation of rainfall and precipitable water over Siberut Island off the western coast of Sumatra Island. *Scientific Online Letters on the Atmosphere*, *4*, 125–128. https://doi.org/10.2151/sola.2008-032

Yamanaka, M., Ogino, S., Wu, P., Hamada, J., Mori, S., Matsumoto, J., & Syamsudin, F. (2018). Maritime Continent coastlines controlling Earth's climate. *Progress in Earth and Planetary Science*, *5*(21), 21. https://doi.org/10.1186/s40645-018-0174-9

Yanase, A., Yasunaga, K., & Masunaga, H. (2017). Relationship between the direction of diurnal rainfall migration and the ambient wind over the Southern Sumatra Island. *Earth and Space Science*, *4*(3), 117–127. https://doi.org/10.1002/2016EA000181

Yang, G.-Y., & Slingo, J. (2001). The diurnal cycle in the tropics. *Monthly Weather Review*, *129*(4), 784–801. https://doi.org/10.1175/1520-0493(2001)129⟨0784:TDCITT⟩2.0.CO;2

Yu, L., Leng, G., & Python, A. (2022). A comprehensive validation for GPM IMERG precipitation products to detect extremes and drought over mainland China. *Weather and Climate Extremes*, *36*, 100458. https://doi.org/10.1016/j.wace.2022.100458